Stem Cell Reports
Article

ISSCR

OPEN ACCESS

Reduced Adult Hippocampal Neurogenesis and Cognitive Impairments following Prenatal Treatment of the Antiepileptic Drug Valproic Acid

Berry Juliandi,[1,2,9] Kentaro Tanemura,[3,9] Katsuhide Igarashi,[4] Takashi Tominaga,[5] Yusuke Furukawa,[6] Maky Otsuka,[4] Noriko Moriyama,[6] Daigo Ikegami,[7] Masahiko Abematsu,[8] Tsukasa Sanosaka,[1] Keita Tsujimura,[1] Minoru Narita,[4,7] Jun Kanno,[6] and Kinichi Nakashima[1,*]

[1]Department of Stem Cell Biology and Medicine, Graduate School of Medical Sciences, Kyushu University, Fukuoka 812-8582, Japan
[2]Department of Biology, Bogor Agricultural University (IPB), Bogor 16680, Indonesia
[3]Laboratory of Animal Reproduction and Development, Graduate School of Agricultural Science, Tohoku University, Miyagi 981-8555, Japan
[4]Life Science Tokyo Advanced Research Center, Hoshi University School of Pharmacy and Pharmaceutical Science, Tokyo 142-8501, Japan
[5]Laboratory of Neural Circuit Systems, Institute of Neuroscience, Kagawa School of Pharmaceutical Sciences, Tokushima Bunri University, Kagawa 769-2193, Japan
[6]Division of Cellular and Molecular Toxicology, Biological Safety Research Center, National Institute of Health Sciences, Tokyo 158-8501, Japan
[7]Department of Pharmacology, Hoshi University School of Pharmacy and Pharmaceutical Science, Tokyo 142-8501, Japan
[8]Department of Orthopaedic Surgery, Graduate School of Medical and Dental Sciences, Kagoshima University, Kagoshima 890-8544, Japan
[9]Co-first author
*Correspondence: kin1@scb.med.kyushu-u.ac.jp
http://dx.doi.org/10.1016/j.stemcr.2015.10.012
This is an open access article under the CC BY-NC-ND license (http://creativecommons.org/licenses/by-nc-nd/4.0/).

SUMMARY

Prenatal exposure to valproic acid (VPA), an established antiepileptic drug, has been reported to impair postnatal cognitive function in children born to VPA-treated epileptic mothers. However, how these defects arise and how they can be overcome remain unknown. Using mice, we found that comparable postnatal cognitive functional impairment is very likely correlated to the untimely enhancement of embryonic neurogenesis, which led to depletion of the neural precursor cell pool and consequently a decreased level of adult neurogenesis in the hippocampus. Moreover, hippocampal neurons in the offspring of VPA-treated mice showed abnormal morphology and activity. Surprisingly, these impairments could be ameliorated by voluntary running. Our study suggests that although prenatal exposure to antiepileptic drugs such as VPA may have detrimental effects that persist until adulthood, these effects may be offset by a simple physical activity such as running.

INTRODUCTION

Epilepsy is one of the most common neurological disorders in the world and is characterized by uncontrollable seizures (Chang and Lowenstein, 2003). Epilepsy can affect anyone, at any age, and there are an estimated 50 million afflicted people worldwide (Meinardi et al., 2001; Ngugi et al., 2010; Joint Epilepsy Council, 2011). The incidence of epilepsy is estimated to be higher than 0.5 cases per 1,000 of population per year (Sander, 2003). Around 30% of sufferers are women of childbearing age (Joint Epilepsy Council, 2011). During pregnancy, epileptic patients must balance the maternal and fetal risks associated with seizures against the potential teratogenicity of antiepileptic drugs (AEDs) (Battino and Tomson, 2007). Although it was recently reported that several commonly used AEDs could produce postnatal impairment of cognitive function if taken during pregnancy (Meador et al., 2009, 2011, 2012, 2013), the precise pathology underlying such impairment remains unknown, and effective treatments for affected children of epileptic mothers who took AEDs during their pregnancy are therefore currently unavailable.

Valproic acid (VPA [2-propylpentanoic acid]) is an established drug in the long-term treatment of epilepsy (Blaheta and Cinatl, 2002). Several studies have revealed that VPA can directly inhibit histone deacetylase (HDAC) activity and cause hyperacetylation of histones, thereby activating gene transcription (Göttlicher et al., 2001; Phiel et al., 2001). VPA significantly impairs postnatal cognitive function (Meador et al., 2009, 2011, 2012, 2013) and can lead to severe developmental defects if taken in early gestational stages (DiLiberti et al., 1984; Nau et al., 1991). We have previously shown, in several culture systems, that VPA enhances neurogenesis and drives neural precursor cells (NPCs) into the neuronal lineage over the glial lineage by a process involving HDAC inhibition (Hsieh et al., 2004; Abematsu et al., 2010; Juliandi et al., 2012). Here, we show that comparable postnatal cognitive functional impairment after prenatal VPA exposure in mice is caused by the untimely enhancement of embryonic neurogenesis, which leads to depletion of the NPCs pool and consequently a decreased level of adult neurogenesis in the hippocampus. We further show that hippocampal neurons in the offspring of VPA-treated mice have an abnormal morphology and activity. Nevertheless, these impairments can be alleviated by voluntary running.

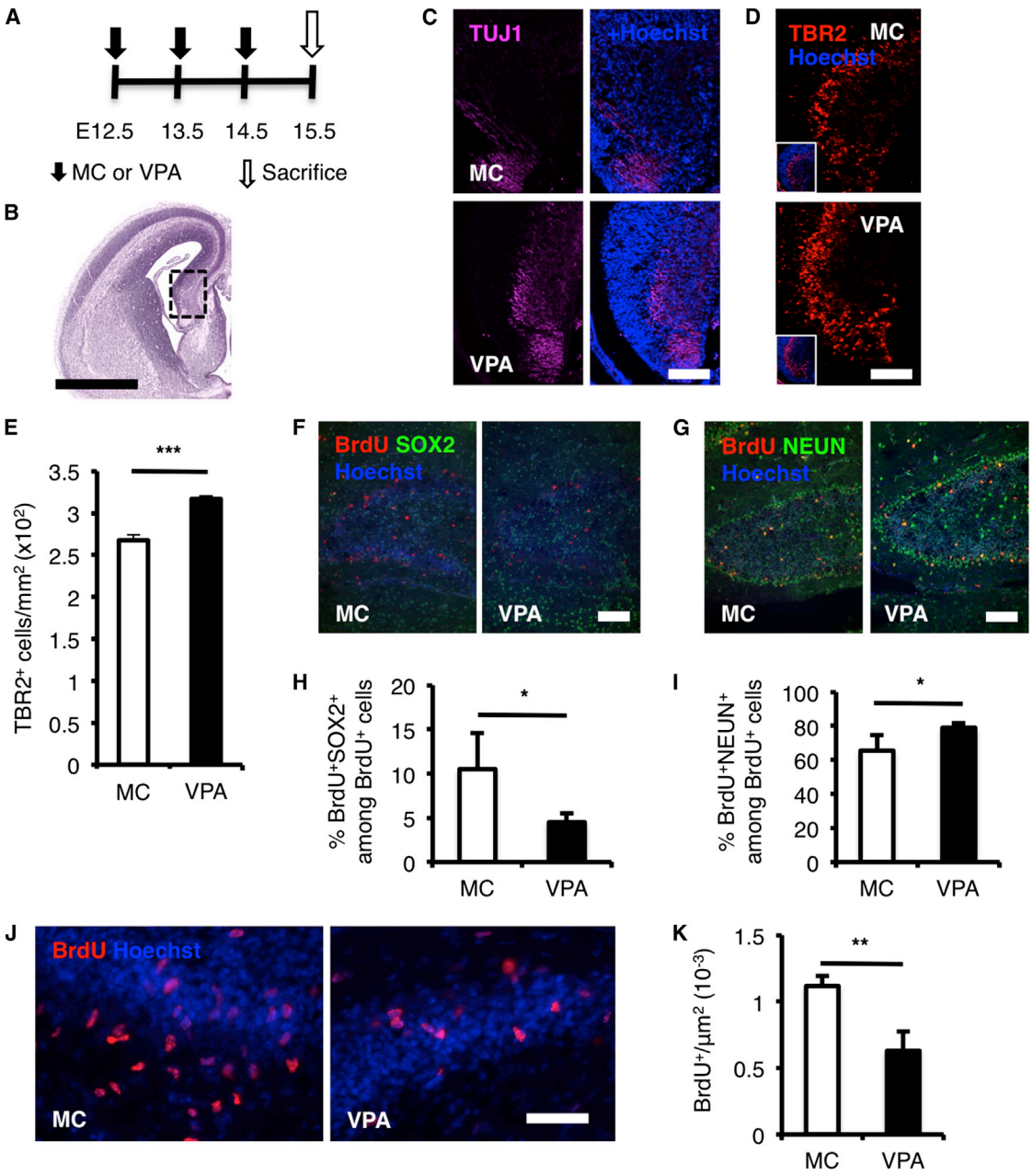

Figure 1. Prenatal VPA Treatment Enhances Untimely Embryonic Neurogenesis

(A) Experimental timeline of prenatal VPA treatment. E, embryonic day.

(B) The region highlighted by the dashed black rectangle in E15.5 forebrain sections was used for analysis in (C) and (D). The image is modified from the Electronic Prenatal Mouse Brain Atlas. Scale bar, 1 mm.

(C) The thickness of the region stained by immature neuron marker β-tubulin isotype III (TUJ1; magenta) is increased in the cortical hem of VPA-treated mice. Scale bar, 100 μm.

(D) VPA treatment increases the production of $TBR2^+$ intermediate neuronal progenitors (red) born in the dentate neuroepithelium. Scale bar, 100 μm.

(E) Quantification of the density of $TBR2^+$ in (D).

(F–I) The proportion of E14.5 BrdU-labeled NPCs (red) expressing NPC marker SOX2 (green; F and H) is reduced, while the ones that had differentiated into $NEUN^+$ neurons are increased at P7 hippocampus after embryonic VPA treatment (green; G and I). Scale bars, 100 μm.

(legend continued on next page)

RESULTS

VPA Enhances Embryonic Neurogenesis and Alters Global Gene Expression through HDAC Inhibition

We orally administered VPA or vehicle (methylcellulose [MC]) to pregnant mice on embryonic day (E)12.5 to E14.5, a mid-gestational period when neurogenesis is prominent (Figure 1A). We found that VPA increased global histone acetylation (Figures S1B–S1D) and enhanced neurogenesis as shown by the increased thickness of TUJ1 stained region in the cortical hem of VPA-treated mice (Figure 1C) and increased production of TBR2-positive intermediate neuronal progenitors born in the dentate neuroepithelium (Figures 1D and 1E) in the developing mouse brain (Figures 1B and S1A; see Figures S1E–S1G for embryonic cortex). We also found that VPA depleted the NPC pool (Figures 1F and 1H, hippocampus; Figures S1E and S1F, cortex) and reduced the number of proliferating NPCs (Figures 1J and 1K, hippocampus; Figures S1H and S1I, cortex). These results were compatible with our previous in vitro observations (Hsieh et al., 2004; Abematsu et al., 2010; Juliandi et al., 2012). Moreover, we found that the fraction of cells that had exited the cell cycle (i.e., differentiated) was higher in the E15.5 forebrain of VPA-treated mice, as shown by an increased number of BrdU-retaining cells that were negative for the proliferation marker KI-67 compared to BrdU-retaining cells that were still KI-67-positive, after a single injection of BrdU on E14.5 to label proliferating cells (Figures S1J and S1K). These results show that VPA treatment enhances embryonic neurogenesis and reduces the pool of NPCs.

Phenotypic changes should be generally induced by gene expression changes, and we wanted to examine whether VPA-induced gene expression change is due to its HDAC inhibiting property. To this end, we administered VPA or valpromide (VPM), an analog AED without HDAC-inhibiting activity, and performed transcriptome analyses at three time points after the final administration. We found that 3 hr after the last administration, global gene expression in the E14.5 telencephalon was changed substantially by VPA, but not by VPM (Figure S1L; GEO: GSE 42904). This global change had almost completely disappeared in both cortex and hippocampus at E18.5 and in hippocampus at P84, although several genes still displayed differential expression levels (Figure S1L). We have found previously that VPM treatment increased neither global histone acetylation nor neurogenesis (Abematsu et al., 2010). Although VPA and VPM might have another pharmacological activity differences beside HDAC-inhibiting activity, taken together our results strongly suggest that VPA alters global gene expression mainly through its HDAC-inhibiting property, and this alteration is short-lived, being restricted mainly to the period when VPA was being given to the mice.

Prenatal VPA Treatment Has the Long-Term Effect of Impairing Adult Neurogenesis, Learning, and Memory

We next investigated whether the enhancement of neurogenesis and changes in gene expression caused by prenatal VPA exposure during the period of prominent neurogenesis could lead to postnatal impairment of cognitive function, as reported in humans (Meador et al., 2009, 2011, 2012, 2013). We conducted several behavioral tests on 12- to 13-week-old male mice (Figure 2A). Although the locomotor activity of VPA-treated mice declined, the decline rate was very slight (Tables S1 and S2) so that we could measure the emotional or cognitive behaviors. We found indeed that VPA-treated mice performed poorly mainly in tests that assessed learning and memory, such as Y-maze (Figure 2B) and contextual and cued fear associative tests (Figures 2C–2E, S4A, S4C, and S4E; Table S1), but not in the other tests (Table S1). VPA-treated mice have a lower correct-arm alternation in Y-maze. VPA-treated mice also have a lower freezing response in contextual and cued fear associative tests than MC-treated mice (control), despite the fact that both groups have similar fear response to foot shock during conditioning (Table S1), indicating that hippocampal-dependent learning and memory (Sarnyai et al., 2000; Van der Borght et al., 2007) are impaired in the VPA-treated mice.

In light of these results, we decided to focus on adult NPCs in the hippocampal dentate gyrus (DG), as they have been shown to play a functional role in learning and memory processes by undergoing neurogenesis to generate adult-born neural cells (Zhao et al., 2008). We injected BrdU once a day for 7 days into 12-week-old mice to label proliferating NPCs in the DG and then sacrificed the mice 1 day (to assess cell proliferation) or 4 weeks (to assess cell survival and fate) after the last BrdU injection (Figure 3A). We found that the number of BrdU-retaining cells in VPA-treated mice was lower at both time points than that in MC-treated control mice (Figures 3B and 3C). We also found fewer proliferating KI-67-positive cells in VPA-treated mice (Figures S2A and S2B). When we traced the fate of BrdU-retaining cells 4 weeks after the last BrdU injection (Figure 3A), we found that a lower proportion

(J and K) Embryonic VPA treatment reduces the number of highly proliferating NPCs (red) labeled by 30 min single-pulse BrdU injection in the P7 DG. See also Figure S1 for other immunostaining data in the cortex of embryonic forebrain.

MC, prenatal methylcellulose (vehicle); VPA, prenatal valproic acid. Data are represented as means. n = 3 for each group. Error bars indicate the SD. *p < 0.05, **p < 0.01, ***p < 0.001, two-tailed t test. Scale bar, 50 μm. See also Figure S1.

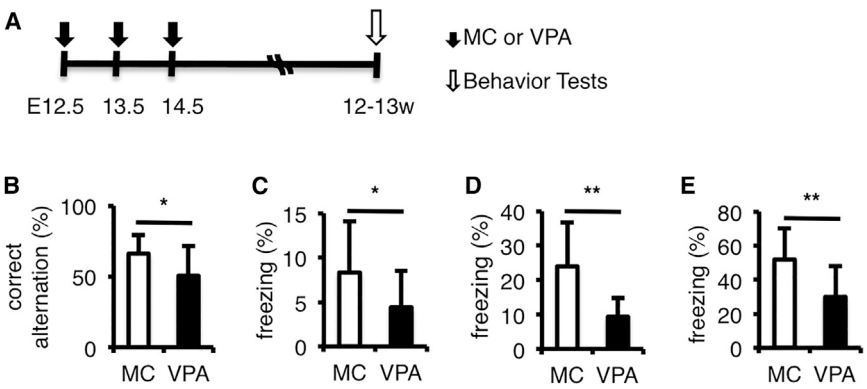

Figure 2. VPA-Treated Mice Perform Poorly in Learning and Memory Tests

(A) Experimental timeline of prenatal VPA treatment and postnatal behavior tests. E, embryonic day; w, weeks old.

(B) VPA-treated mice have a lower correct-arm alternation than MC-treated mice (control).

(C–E) VPA-treated mice have a lower freezing response than MC-treated mice (control) in conditioning (C; day 1), contextual (D; day 2), and cued fear associative tests (E; day 3). See also Figures S4A, S4C, and S4E for time course of freezing response and Table S1 for a summary of behavior data.

MC, prenatal methylcellulose (vehicle); VPA, prenatal valproic acid. Data are represented as means. n = 12 for each group. Error bars indicate the SD. *p < 0.05, **p < 0.01, two-tailed t test. See also Figure S4 and Table S1.

of BrdU-retaining cells had differentiated into NEUN-positive neurons and S100β-positive astrocytes in VPA-treated mice than in MC-treated mice (Figure 3D). The possibility that more BrdU-retaining cells had died in VPA-treated mice during the 4-week period can be ruled out, because the survival rate of BrdU-retaining cells in these mice was similar to that in MC-treated mice (Figure 3E). These results imply that BrdU-retaining cells in VPA-treated mice either differentiated to another cell type(s) or differentiated more slowly than those in MC-treated mice. The latter explanation is more plausible, because we found that a higher proportion of BrdU-retaining cells in VPA-treated mice still expressed SOX2 (an NPC marker) and KI-67 (a proliferation marker) even 4 weeks after the last BrdU injection (Figures S2C–S2E). We also found that 1 day after the last BrdU injection, almost all BrdU-positive cells were still KI-67-positive in VPA-treated mice, whereas several BrdU-positive but KI-67-negative cells already existed in MC-treated mice (Figure S2F). We also examined amygdala and cortex, other brain regions that were suggested to play important roles in the regulation of memory and fear associative responses (LeDoux, 2003; van Strien et al., 2009). It has been shown previously that amygdala volume associates with differences in fear associative responses (Yang et al., 2008). However, we found that VPA-treated mice have a similar amygdala size to that of MC-treated mice, both at P7 and P84 (Figures S3A–S3D). We also found no significant difference in the expression level of cortical layer-specific genes such as *Cux1*, *Satb2*, and *Ctip2* (Molyneaux et al., 2007) in the cortex of P84 VPA-treated mice (Figures S3E–S3G). Taken together, these results suggest that prenatal VPA treatment has the long-term effect of impairing adult neurogenesis and contribute to the poor performance of VPA-exposed mice in learning and memory tests.

Voluntary Running Restores Learning and Memory Deficiencies in VPA-Treated Mice, Probably through Increased Neurogenesis that Yields Neurons with Normal Morphology

Voluntary running can increase adult neurogenesis in the hippocampal DG (van Praag et al., 1999a, 1999b). We next provided the mice with a running wheel (RW) after they had weaned and repeated the same BrdU-injection experiment when they reached 12 weeks (P84; Figure 3A). We observed an increased number of BrdU-retaining cells in MC- and VPA-treated mice with the RW, both 1 day and 4 weeks after the last BrdU injection (Figures 4A and 4B). We also found an increased proportion of BrdU-retaining cells that had differentiated into NEUN-positive neurons and a reduced proportion of BrdU-retaining cells that still SOX2-positive in MC- and VPA-treated mice with the RW, 4 weeks after the last BrdU injection (Figures 3A, 4C, and 4D). Voluntary running also enabled VPA-treated mice to perform better in hippocampus-dependent learning and memory test, the correct alternation in Y-maze ($F(1, 13) = 22.74$, $p < 0.001$, one-way ANOVA), and this performance was not significantly different in comparison to MC-treated mice (Figure 4E; Table S2). Moreover, we found that voluntary running also led VPA-treated mice performing better in conditioning ($F(1, 13) = 3.06$, $p = 0.10$, one-way ANOVA) and cued fear tests ($F(1, 13) = 6.80$, $p < 0.05$, one-way ANOVA), although not in contextual fear test ($F(1, 13) = 0.47$, $p = 0.50$, one-way ANOVA). As each mouse showed similar normal fear response, the performance of VPA-treated mice after voluntary running in conditioning and cued fear tests, but not in contextual fear test, recovered to levels that were not significantly different from that of MC-treated mice (Figures 4F–4H, S4B, S4D, and S4F; Table S2). However, when we analyzed all experimental groups by two-way ANOVA with both

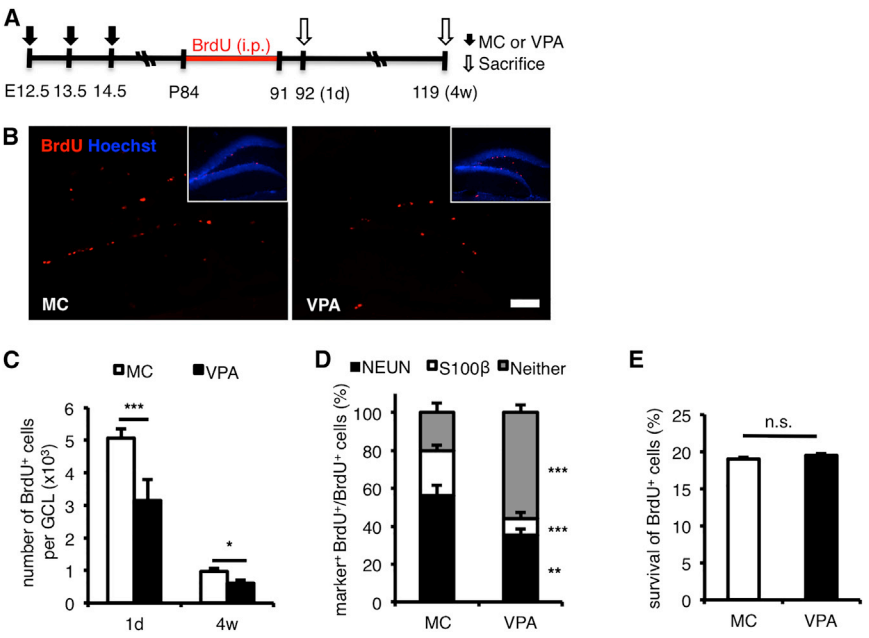

Figure 3. Prenatal VPA Treatment Has the Long-Term Effect on the Adult Neurogenesis

(A) Experimental timeline of prenatal VPA treatment and adult neurogenesis analysis. E, embryonic day; P, postnatal day; 1d, 1 day after the last intraperitoneal (i.p.) BrdU injection; 4w, 4 weeks after the last i.p. BrdU injection.

(B) Representative images of brain sections including the hippocampal DG stained for BrdU (red) and with Hoechst 33258 (blue),1 day after the last BrdU injection. See also Figure S2A for KI-67 staining.

(C) Quantification of $BrdU^+$ cells in the granule cell layer (GCL), 1 day (1d; n = 8 for each group) and 4 weeks (4w; n = 8 for each group) after the last BrdU injection, shows a reduction of $BrdU^+$ cells in the hippocampus. See also Figure S2B for quantification of KI-67$^+$ cells in the GCL.

(D) NPC differentiation into $NEUN^+$ neurons and $S100\beta^+$ astrocytes is impaired in VPA-treated mice, as shown by a reduced proportion of marker-positive and $BrdU^+$ cells among total $BrdU^+$ cells at 4 weeks after the last BrdU injection (n = 4 for each group).

(E) $BrdU^+$ cell survival is similar in VPA- and MC-treated mice. Quantification of $BrdU^+$ cell survival in each group as a percentage of $BrdU^+$ cells at 4w relative to $BrdU^+$ cells at 1d (n = 8 for each group).

MC, prenatal methylcellulose (vehicle); VPA, prenatal valproic acid. Data are represented as means. Error bars indicate the SD. *p < 0.05, **p < 0.01, ***p < 0.001, n.s., not significantly different, two-tailed t test. Scale bar, 100 μm. See also Figures S2 and S3.

prenatal treatment and postnatal activity as factors, the results did not show a significant effect of postnatal activity on the performance of mice in hippocampus-dependent learning and memory tests (Table S2). This is mainly because voluntary running in MC-treated mice made no significant contribution to the performance in hippocampus-dependent learning and memory tests (conditioning: $F(1, 13) = 0.13$, $p = 0.72$; contextual: $F(1, 13) = 0.26$, $p = 0.62$; cued: $F(1, 13) = 0.01$, $p = 0.93$; Y-maze: $F(1, 13) = 1.17$, $p = 0.30$; one-way ANOVA). In addition, we found no significant interaction between prenatal drug treatment and postnatal activity in relation to the behavior of mice, except for the correct alternation in Y-maze ($F(1, 26) = 5.59$, $p < 0.05$, two-way ANOVA; Table S2). Therefore, it seems likely that only a certain level of adult neurogenesis is required for mice to perform normally in these hippocampus-dependent learning and memory tests, so that MC-treated mice with or without a RW showed no significant differences in these tests even though MC-treated mice with a RW displayed higher levels of neurogenesis than those without one. However, because the level of adult neurogenesis in the VPA-treated mice was below this threshold, the mice performed poorly in these tests; voluntary running improved their performance, probably by increasing adult neurogenesis in the hippocampus to above the threshold level.

We next sought to determine whether adult neurogenesis in the DG of VPA-treated mice generated normal or abnormal neurons. We found that DCX-positive immature neurons (Figures 5A and S5A) and Golgi-stained mature neurons (Figures 5B and S5B) in the DG of VPA-treated mice displayed an abnormal morphology with shorter total dendritic length (Figures 5D and 5E) and fewer dendrite processes toward the molecular layer, as shown by a wider maximum dendritic span compared to MC-treated mice (Figure 5G). The dendritic complexity of Golgi-stained neurons in VPA-treated mice, however, was similar to that of MC-treated mice (Figures 5F and S5B). Surprisingly, this abnormal morphology could also be overcome by voluntary running (Figures 5A, 5B, 5D, 5E, 5G, S5A, and S5B). Taken together, these observations suggest that the restoration of learning and memory deficiencies in VPA-treated mice through running is involved in increased neurogenesis, which gives rise to neurons with normal morphology.

Several mechanisms have been proposed to be responsible for the voluntary running-induced increase in adult hippocampal neurogenesis. Voluntary running can induce expression of neurotrophic factors such as *brain-derived neurotrophic factor* (*Bdnf*) in the hippocampus (van Praag,

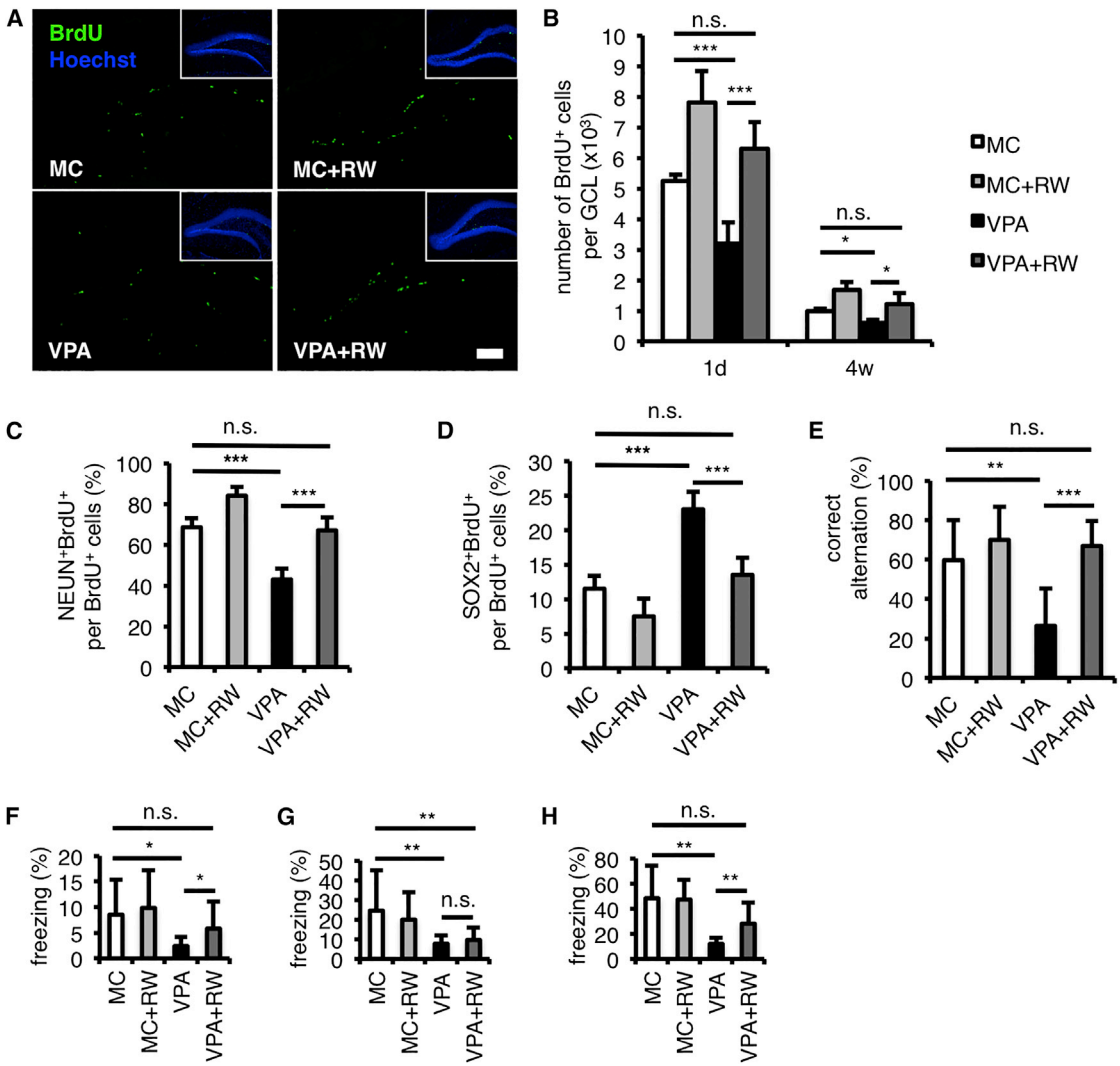

Figure 4. Voluntary Running Restores Adult Neurogenesis and Cognitive Deficiencies of VPA-Treated Mice

(A) Representative images of brain sections including the hippocampal DG stained for BrdU (green) and with Hoechst 33258 (blue), 1 day after the last BrdU injection. See Figure 2A for the experimental timeline.

(B) Quantification of $BrdU^+$ in the granule cell layer (GCL), 1 day (1d; n = 8 for each group) and 4 weeks (4w; n = 8 for each group) after the last BrdU injection, shows an increased number of $BrdU^+$ cells in the hippocampus after voluntary running.

(C and D) Voluntary running recovers the proportion of $BrdU^+$ cells that had differentiated into $NEUN^+$ neurons (C) and the ones that still expressed SOX2 (D) among total $BrdU^+$ cells at 4 weeks after the last BrdU injection (n = 4 for each group).

(E) Reduction of correct-arm alternation in Y-maze tests of VPA-treated mice is recovered by voluntary running (n = 7 for MC and VPA + RW; n = 8 for MC + RW and VPA).

(F–H) Voluntary running recovers the freezing response in conditioning (F; day 1) and in cued fear associative tests (H; day 3), but not in contextual fear associative tests (G; day 2; n = 7 for MC and VPA + RW; n = 8 for MC + RW and VPA). See also Figures S4B, S4D, and S4F for the time course of the freezing response and Table S2 for a summary of behavior data.

MC, prenatal methylcellulose (vehicle); MC + RW, prenatal methylcellulose and postnatal running; VPA, prenatal valproic acid; VPA + RW, prenatal valproic acid and postnatal running. Data are represented as means. Error bars indicate the SD. *p < 0.05, **p < 0.01, ***p < 0.001, n.s., not significantly different, two-tailed t test. Scale bar, 100 μm. See also Figure S4 and Table S2.

2009; Farmer et al., 2004), and *Bdnf* has been suggested to have an important role in adult neurogenesis, neuronal maturation, and dendrite arborization (Tolwani et al., 2002; Bekinschtein et al., 2011; Stranahan, 2011). Indeed, we found an increased level of *Bdnf* expression after running in both MC- and VPA-treated mice hippocampus

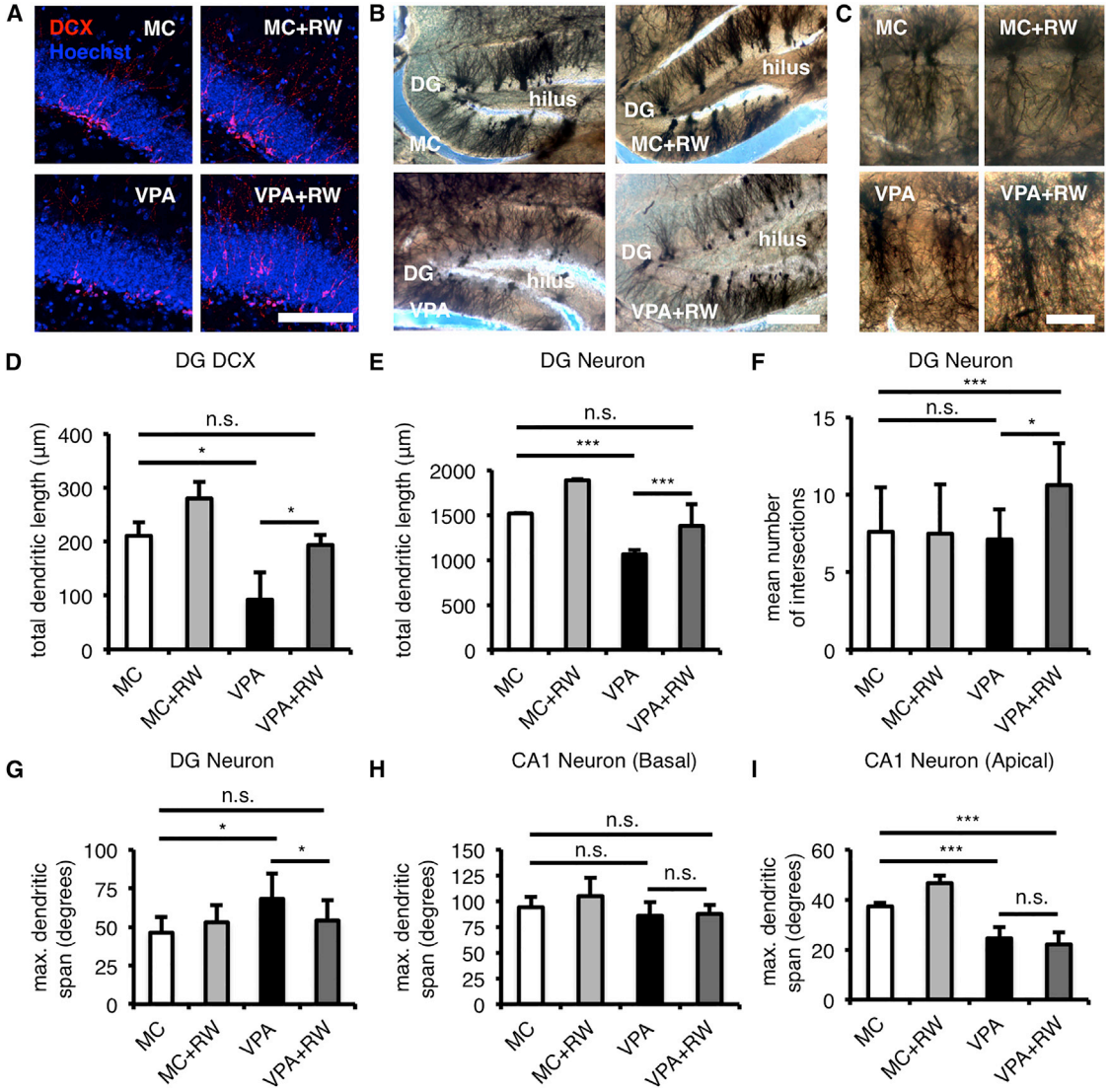

Figure 5. Voluntary Running Restores Neuronal Morphology in VPA-Treated Mice

(A) Impaired morphology of DCX$^+$ young neurons in the DG of VPA-treated mice is recovered by voluntary running (n = 4 for each group). Scale bar, 100 μm.

(B) Impaired morphology of Golgi-Cox stained neurons in the DG of VPA-treated mice is recovered by voluntary running (n = 3 for each group). Note that voluntary running recovered non-molecular layer-oriented dendrites in VPA-treated mice to molecular layer-oriented ones. Scale bar, 100 μm.

(C) Impaired morphology of Golgi-Cox stained neurons in the CA1 of VPA-treated mice is not recovered by voluntary running (n = 3 for each group). Note that the less-ramified and straighter apical dendrites in VPA-treated mice could not be recovered by voluntary running. Scale bar, 50 μm.

(D–F) Voluntary running recovers total dendritic length of DCX$^+$ young neurons (D) and Golgi-Cox stained neurons (E) and increases dendritic complexity of Golgi-Cox stained neurons (F) in the DG of VPA-treated mice. See also Figures S5A and S5B for Sholl analysis.

(G–I) Abnormal dendritic span of DG neurons (G), but not of apical dendritic span of CA1 neurons (I), is recovered by voluntary running in VPA-treated mice, while basal dendrites of CA1 neurons show similar dendritic span across groups (H).

MC, prenatal methylcellulose (vehicle); MC + RW, prenatal methylcellulose and postnatal running; VPA, prenatal valproic acid; VPA + RW, prenatal valproic acid and postnatal running. Data are represented as means. Error bars indicate the SD. *p < 0.05, ***p < 0.001, n.s., not significantly different, two-tailed t test. See also Figure S5.

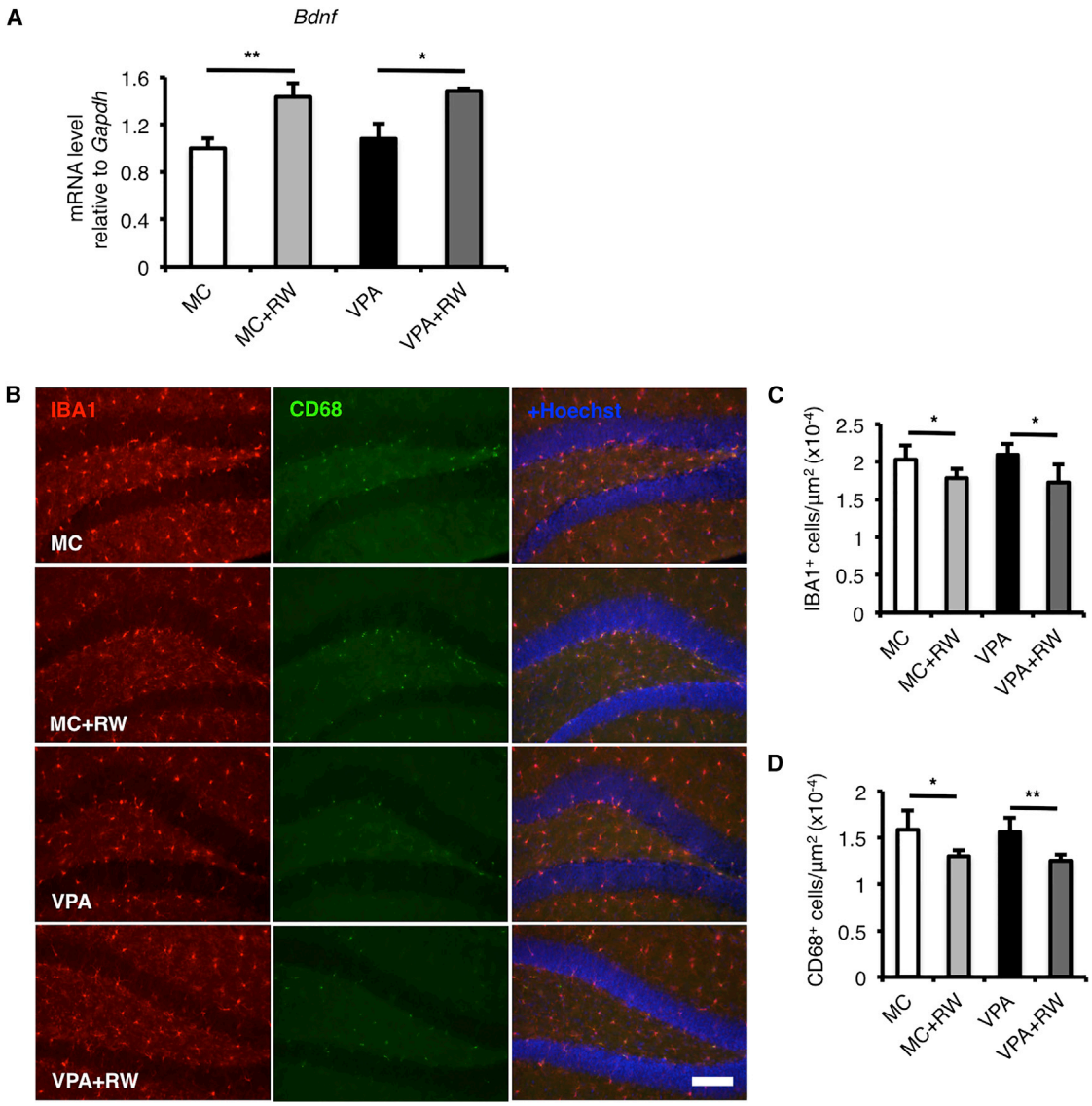

Figure 6. Voluntary Running Increases the *Bdnf* Expression Level and Reduces Microglia and Activated Microglia in the Hippocampus

(A) The expression level of *brain-derived neurotrophic factor* (*Bdnf*) was increased by voluntary running in both MC- and VPA-treated mice. (B–D) Voluntary running reduced the number of IBA1$^+$ microglia (red; B and C) and CD68$^+$-activated microglia (green; B and D) in both MC- and VPA-treated mice.

MC, prenatal methylcellulose (vehicle); MC + RW, prenatal methylcellulose and postnatal running; VPA, prenatal valproic acid; VPA + RW, prenatal valproic acid and postnatal running; *Gapdh*, *glyceraldehyde 3-phosphate dehydrogenase*. Data are represented as means. n = 3 for each group. Error bars indicate the SD. *p < 0.05, **p < 0.01, two-tailed t test. Scale bar, 100 μm.

(Figure 6A). Voluntary running has also been shown to reduce the number of microglia and its activation (Gebara et al., 2013; Kohman et al., 2013), and previous reports showed that microglia can suppress the adult hippocampal neurogenesis (Sierra et al., 2010; Vukovic et al., 2012; Matsuda et al., 2015). Interestingly, we found that the number of IBA1-positive microglia and CD68-positive-activated microglia was also decreased by voluntary running in both MC- and VPA-treated mice (Figures 6B–6D). Therefore, it is plausible that voluntary running helped VPA-treated mice through the increased adult hippocampal neurogenesis that was caused by the increase level of *Bdnf* expression and the reduction of microglia and its activated form in the hippocampus.

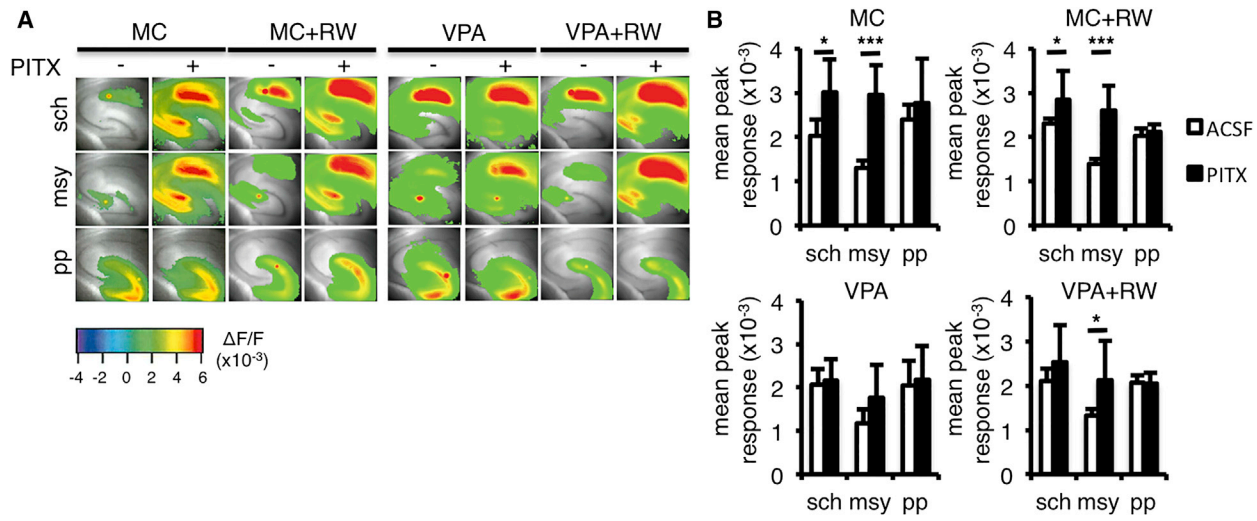

Figure 7. Voluntary Running Restores Neuronal Activity in VPA-Treated Mice

(A) Representative pseudocolor activity map images of brain slices including the hippocampus show that voluntary running can only recover the impairment of $GABA_A$ receptor-mediated inhibition in the mossy fiber pathway (msy) of VPA-treated mice, after treatment with the $GABA_A$ receptor channel antagonist picrotoxin (PITX) (n = 6 for MC, n = 9 for MC + RW, n = 7 for VPA, n = 8 for VPA + RW). Electrical stimulation was applied to Schaffer collateral afferents at the CA3/CA1 border of CA1 (sch); to the granule cell layer to stimulate the mossy fiber pathway (msy); and to the molecular layer of the upper blade in the DG (pp).

(B) Quantification of the neural response in artificial cerebrospinal fluid (ACSF), with (black bars) or without PITX (white bars; n = 6 for MC, n = 9 for MC + RW, n = 7 for VPA, n = 8 for VPA + RW). Note that although the augmentation of the neural response caused by $GABA_A$ receptor-mediated inhibition with PITX application seen in sch and msy was abolished in VPA-treated mice, voluntary running could restore the augmentation only in the msy.

MC, prenatal methylcellulose (vehicle); MC + RW, prenatal methylcellulose and postnatal running; VPA, prenatal valproic acid; VPA + RW, prenatal valproic acid and postnatal running. Data are represented as means. Error bars indicate the SD. *$p < 0.05$, ***$p < 0.001$, two-tailed t test.

Voluntary Running Cannot Mitigate Abnormal Neuronal Morphology or Function of the Hippocampal CA1 Region in VPA-Treated Mice

The freezing response in the contextual fear test after voluntary running by VPA-treated mice did not recover to the level displayed by MC-treated mice (Figures 4G and S4D; Table S2). It has been proposed that recall of contextual memories relies more on CA1 than other regions in the hippocampus (Hall et al., 2001). Indeed, we found that apical dendrite morphology was abnormal in CA1 neurons of VPA-treated mice, and this defect was not repaired by voluntary running (Figures 5C, 5H, and 5I). Moreover, when we examined the region-specific restoration by voluntary running of neuronal activity in the hippocampus, the basal neuronal responses upon electrical stimulation were not affected by VPA nor voluntary running in the three major synaptic connections in the hippocampus (CA3-CA1, Schaffer collateral afferent [sch]; DG-CA3, mossy fiber [msy]; EC-DG, perforant pathway [pp]) possibly due to some homeostatic balancing mechanism (Turrigiano and Nelson, 2004; Turrigiano, 2011). However, when the excitatory activity was measured, with the increase in activity caused by an inhibitor for $GABA_A$ receptor picrotoxin (PITX) application, the effect of VPA became apparent. That is, the PITX induced an increase in sch and msy in MC-treated mice, which was not seen in VPA-treated mice, suggesting the impairment of inhibitory action in VPA-mice. The voluntary running could restore the characteristics only in msy (Figure 7). These results may explain why the recovery of neurogenesis and neuronal morphology of the DG in VPA-treated mice could not ameliorate their poor performance in the contextual associative test. Previous studies have indicated that ablation of adult neurogenesis in the DG leads to defective performance in a contextual associative test (Saxe et al., 2006; Wojtowicz et al., 2008) (but see Shors et al., 2002), but enhanced neurogenesis or running was weakly related to the performance in the test (Wojtowicz et al., 2008).

DISCUSSION

The precise pathology underlying postnatal impairment of cognitive function in children of epileptic expectant mothers treated with VPA, commonly used AED, is

unknown. Based on our findings in mice, we propose that the impairment is attributable to the untimely enhancement of embryonic neurogenesis, which leads to depletion of the NPC pool and consequently to a decreased level of postnatal neurogenesis in the hippocampus. Children of epileptic expectant mothers treated with VPA may also have hippocampal neurons with abnormal morphology and activity, as were observed in this study. Although prenatal exposure to AEDs such as VPA may have detrimental effects that persist until adulthood, we suggest that these effects could be mitigated by a simple physical activity such as running. Our results thus offer a straightforward strategy to help children born to epileptic mothers.

The cognitive deficits associated with prenatal VPA exposure might not due solely to the reduced neurogenesis with the abnormal neuronal morphology in the hippocampus, and there is a possibility that the low freezing responses in fear associative tests were contributed by the deficiency in amygdala, nociception, and/or motoric functions. Nevertheless, our data suggested that the reduced neurogenesis associated with the abnormal neuronal morphology in the hippocampus were very likely to be correlated with the observed cognitive deficits for several reasons. First, voluntary running is well known for its effect on enhancing both adult neurogenesis in the DG of the hippocampus and hippocampus-dependent learning and memory (Zhao et al., 2008), and this voluntary running could recover the cognitive deficit, if not all, in VPA-treated mice with reduced neurogenesis in the DG. Second, to the best of our knowledge, there are no reports to date that show a direct contribution of voluntary running to the enhancement of amygdala function that subsequently leads to an improvement in the cued fear response. Third, based on experiments that we have conducted, we could not find any significant differences in amygdala size and in the expression levels of cortical layer-specific genes of MC- and VPA-treated mice, with or without voluntary running. Fourth, total traveled distance in the open field, elevated plus and the Y-maze tests, and the number of light/dark transitions were not significantly different between MC- and VPA-treated mice, although in our earlier experiment some of these parameters showed modest differences. Moreover, in fear associative test, VPA-treated mice move similarly to MC-treated mice before the start of the tone (pre-tone), which indicate that motor deficiency is unlikely to be the main cause of low freezing responses in VPA-treated mice. Fifth, MC- and VPA-treated mice have similar basal nociceptive response and startle response to electric footshock during the conditioning for fear-associative test, thus it seems unlikely that VPA-treated mice have abnormal nociception and cannot sense the foot shock. Taking these facts into consideration, we therefore suggested that the reduced neurogenesis associated with the abnormal neuronal morphology in the hippocampus were very likely to be a critical cause of the observed cognitive deficits. However, we still cannot completely exclude the possibility that changes in other brain areas may also contribute to the deficits, warranting further future investigation.

We and others have shown previously that VPA treatment induces neuronal differentiation but suppresses glial differentiation of cultured multipotent NPCs (Hsieh et al., 2004; Balasubramaniyan et al., 2006; Murabe et al., 2007; Abematsu et al., 2010; Juliandi et al., 2012). We have now demonstrated that VPA also increases histone acetylation in the embryonic forebrain and induces neuronal differentiation of embryonic NPCs. Previous study have shown that VPA promotes neuronal differentiation by increasing histone H4 acetylation at proneural gene promoters (Yu et al., 2009). However, several studies have suggested that the activation of GSK-3β/β-catenin and/or ERK pathway is the main cause for the increase neurogenesis of NPCs by VPA (Yuan et al., 2001; Jung et al., 2008; Hao et al., 2004; Go et al., 2012). It has been suggested that VPA might have various cellular effects that will depend on the context of VPA usage and/or cell type and experimental design used in the study, which warrant further research to reveal the connection between these effects (Kostrouchová et al., 2007; Rosenberg, 2007).

We suggest that gene expression change caused by VPA is attributable mainly to its HDAC-inhibiting activity. To date, more than a dozen HDACs have been characterized and they are classified into at least three major groups. In particular, HDAC1 and HDAC2, belonging to the class I group, have been reported to regulate NPC differentiation (Sun et al., 2011). NPCs express high levels of HDAC1 and some of them also express low levels of HDAC2 (MacDonald and Roskams, 2008). Interestingly, as NPCs are committed to the neuronal lineage, expression of HDAC2 is upregulated while that of HDAC1 is downregulated and becomes undetectable in most post-mitotic neurons (MacDonald et al., 2005; MacDonald and Roskams, 2008); on the other hand, HDAC1 expression is sustained in the majority of cells in glial lineages (astrocytes and oligodendrocytes), in which HDAC2 is not detected (Shen et al., 2005; MacDonald and Roskams, 2008). Moreover, HDAC2, but not HDAC1, was found to inhibit astrocytic differentiation (Humphrey et al., 2008). Therefore, although VPA is capable of inhibiting both HDAC1 and HDAC2 (Kazantsev and Thompson, 2008), it is tempting to speculate that the main target of VPA in HDAC inhibition-mediated neuronal differentiation of NPCs is HDAC1. It will be of interest to explore this possibility in a future study.

Neurogenesis in the adult mammalian brain occurs throughout life and has been clearly demonstrated at two

locations under physiological conditions: the SVZ of the lateral ventricle and the subgranular zone (SGZ) of the DG in the hippocampus (Alvarez-Buylla and Lim, 2004). Several studies have shown that hippocampal neurogenesis is regulated by both physiological and pathological activities at different stages, including (1) proliferation of NPCs, (2) fate determination and differentiation of NPCs, and (3) survival, maturation, and integration of newborn neurons (Zhao et al., 2008). Furthermore, each of these stages is subject to regulation by numerous intrinsic and extrinsic factors (Suh et al., 2009). Genetic and environmental factors that affect adult hippocampal neurogenesis also cause alteration in cognitive performance, suggesting roles for adult hippocampal neurogenesis in learning and memory (Zhao et al., 2008). Our results showed that VPA-treated mice have a decreased level of postnatal neurogenesis in the hippocampus, which correlates with their poor performance in learning and memory tests. We have shown here and elsewhere (Hsieh et al., 2004; Jessberger et al., 2007) that VPA can reduce the proliferation of NPCs, and this reduction, together with the enhancement of neurogenesis, probably led to the depletion of the NPC pool in VPA-treated mice. It is possible that this depletion caused a slower differentiation of the residual NPCs in order to maintain required number of NPC pool during life. This possibility is an interesting avenue to be explored in the future.

In accordance with previous studies (van Praag et al., 1999a, 1999b), we found that voluntary running augments hippocampal neurogenesis of both MC- and VPA-treated mice, and it restores learning and memory deficiencies in VPA-treated mice. A previous report has shown the same restoration of decreased hippocampal neurogenesis and learning deficits in aged rodents by voluntary running (van Praag et al., 2005), although the precise molecular mechanisms responsible for voluntary running-induced neurogenesis remain undetermined (Deng et al., 2010). Here, we propose that at least the increase expression level of *Bdnf*, and the reduction of activated microglia may contribute to the restoration of impaired hippocampal neurogenesis and neuronal morphology in the DG of VPA-treated mice after voluntary running. However, future exploration is necessary to reveal the direct connection between the increase expression level of *Bdnf* and the reduction of microglia and its activated form in the hippocampus after voluntary running.

EXPERIMENTAL PROCEDURES

Animal Treatment

All experiments were carried out according to institutional animal experimentation guidelines, which comply with the NIH Guide for Care and Use of Laboratory Animals. All efforts were made to minimize the number of animals used and their suffering. Pregnant C57BL/6 mice were individually housed in plastic breeding cages with free access to water and pellet diet in a 12-hr light-dark cycle. For a detailed description of groups and treatments, see the Supplemental Experimental Procedures.

Immunohistochemistry, Nissl, and Golgi Staining

Mice were anesthetized and perfused with PBS followed by 4% PFA in PBS. The brain was dissected, postfixed, and processed for immunohistochemistry. For Nissl staining, brain sections were defatted with xylene, hydrated through a graded ethanol series (100%, 95%, and 70%), and washed with water before stained with 0.2% thionin solution (pH 4.0). Sections were then dehydrated in water and a graded ethanol series (70%, 95%, and 100%), clear in xylene, and mounted with Entellan (Merck). For Golgi staining, the brain was removed from the skull without any perfusion and then sectioned (100 μm) on a cryostat. For a more detailed description and list of antibodies, see the Supplemental Experimental Procedures.

Measurement and Morphometrics

For a detailed description of cell count, volume measurement and cell/tissue morphometrics, see the Supplemental Experimental Procedures.

Gene Expression Analysis

For a detailed description of GeneChip and real-time qPCR procedures, see the Supplemental Experimental Procedures.

Behavioral Tests

Behavioral experiments were performed sequentially using male mice. For a more detailed description, see the Supplemental Experimental Procedures.

Voltage-Sensitive Dye Imaging

Experiment was done using hippocampal slices. For a more detailed description, see the Supplemental Experimental Procedures.

Statistics

Statistical analyses were performed by Student's two-tailed t test (unpaired) and one-way or two-way ANOVA using R software (http://www.r-project.org) (n indicates individual mice).

ACCESSION NUMBERS

The accession number for the GeneChip data reported in this paper is GEO: GSE42904.

SUPPLEMENTAL INFORMATION

Supplemental Information includes Supplemental Experimental Procedures, five figures, and two tables and can be found with this article online at http://dx.doi.org/10.1016/j.stemcr.2015.10.012.

AUTHOR CONTRIBUTIONS

B.J. and K.N. conceived and designed the study. B.J., K. Tanemura, K.I., T.T., Y.F., M.O.I., N.M., and D.I. carried out the experiments. B.J., K. Tanemura, K.I., T.T., M.A., T.S., K. Tsujimura, M.N., and K.N. analyzed the data. J.K. supported the experiments. B.J. and K.N. wrote the manuscript.

ACKNOWLEDGMENTS

We thank Y. Bessho, T. Matsui, Y. Nakahata, J. Kohyama, T. Takizawa, M. Namihira, S. Katada, and T. Imamura for valuable discussions. We also thank I. Smith for critical reading of the manuscript. We are very grateful to M. Tano for her excellent secretarial assistance and other laboratory members for discussion and technical help. This research was supported in part by the NAIST Global COE Program (Frontier Biosciences: Strategies for survival and adaptation in a changing global environment) from the Ministry of Education, Culture, Sports, Science and Technology of Japan (MEXT); a Grant-in-Aid for Scientific Research on Innovative Area: Neural Diversity and Neocortical Organization from MEXT; Health Sciences Research Grants from the Ministry of Health, Labour and Welfare, Japan; Core Research for Evolutional Science and Technology (CREST) from the Japan Science and Technology Corporation; and Research Fellowships for Young Scientists from the Japan Society for the Promotion of Science.

Received: June 24, 2015
Revised: October 22, 2015
Accepted: October 23, 2015
Published: November 19, 2015

REFERENCES

Abematsu, M., Tsujimura, K., Yamano, M., Saito, M., Kohno, K., Kohyama, J., Namihira, M., Komiya, S., and Nakashima, K. (2010). Neurons derived from transplanted neural stem cells restore disrupted neuronal circuitry in a mouse model of spinal cord injury. J. Clin. Invest. *120*, 3255–3266.

Alvarez-Buylla, A., and Lim, D.A. (2004). For the long run: maintaining germinal niches in the adult brain. Neuron *41*, 683–686.

Balasubramaniyan, V., Boddeke, E., Bakels, R., Küst, B., Kooistra, S., Veneman, A., and Copray, S. (2006). Effects of histone deacetylation inhibition on neuronal differentiation of embryonic mouse neural stem cells. Neuroscience *143*, 939–951.

Battino, D., and Tomson, T. (2007). Management of epilepsy during pregnancy. Drugs *67*, 2727–2746.

Bekinschtein, P., Oomen, C.A., Saksida, L.M., and Bussey, T.J. (2011). Effects of environmental enrichment and voluntary exercise on neurogenesis, learning and memory, and pattern separation: BDNF as a critical variable? Semin. Cell Dev. Biol. *22*, 536–542.

Blaheta, R.A., and Cinatl, J., Jr. (2002). Anti-tumor mechanisms of valproate: a novel role for an old drug. Med. Res. Rev. *22*, 492–511.

Chang, B.S., and Lowenstein, D.H. (2003). Epilepsy. N. Engl. J. Med. *349*, 1257–1266.

Deng, W., Aimone, J.B., and Gage, F.H. (2010). New neurons and new memories: how does adult hippocampal neurogenesis affect learning and memory? Nat. Rev. Neurosci. *11*, 339–350.

DiLiberti, J.H., Farndon, P.A., Dennis, N.R., and Curry, C.J. (1984). The fetal valproate syndrome. Am. J. Med. Genet. *19*, 473–481.

Farmer, J., Zhao, X., van Praag, H., Wodtke, K., Gage, F.H., and Christie, B.R. (2004). Effects of voluntary exercise on synaptic plasticity and gene expression in the dentate gyrus of adult male Sprague-Dawley rats in vivo. Neuroscience *124*, 71–79.

Gebara, E., Sultan, S., Kocher-Braissant, J., and Toni, N. (2013). Adult hippocampal neurogenesis inversely correlates with microglia in conditions of voluntary running and aging. Front. Neurosci. *7*, 145.

Go, H.S., Kim, K.C., Choi, C.S., Jeon, S.J., Kwon, K.J., Han, S.H., Lee, J., Cheong, J.H., Ryu, J.H., Kim, C.H., et al. (2012). Prenatal exposure to valproic acid increases the neural progenitor cell pool and induces macrocephaly in rat brain via a mechanism involving the GSK-3β/β-catenin pathway. Neuropharmacology *63*, 1028–1041.

Göttlicher, M., Minucci, S., Zhu, P., Krämer, O.H., Schimpf, A., Giavara, S., Sleeman, J.P., Lo Coco, F., Nervi, C., Pelicci, P.G., and Heinzel, T. (2001). Valproic acid defines a novel class of HDAC inhibitors inducing differentiation of transformed cells. EMBO J. *20*, 6969–6978.

Hall, J., Thomas, K.L., and Everitt, B.J. (2001). Cellular imaging of zif268 expression in the hippocampus and amygdala during contextual and cued fear memory retrieval: selective activation of hippocampal CA1 neurons during the recall of contextual memories. J. Neurosci. *21*, 2186–2193.

Hao, Y., Creson, T., Zhang, L., Li, P., Du, F., Yuan, P., Gould, T.D., Manji, H.K., and Chen, G. (2004). Mood stabilizer valproate promotes ERK pathway-dependent cortical neuronal growth and neurogenesis. J. Neurosci. *24*, 6590–6599.

Hsieh, J., Nakashima, K., Kuwabara, T., Mejia, E., and Gage, F.H. (2004). Histone deacetylase inhibition-mediated neuronal differentiation of multipotent adult neural progenitor cells. Proc. Natl. Acad. Sci. USA *101*, 16659–16664.

Humphrey, G.W., Wang, Y.H., Hirai, T., Padmanabhan, R., Panchision, D.M., Newell, L.F., McKay, R.D., and Howard, B.H. (2008). Complementary roles for histone deacetylases 1, 2, and 3 in differentiation of pluripotent stem cells. Differentiation *76*, 348–356.

Jessberger, S., Nakashima, K., Clemenson, G.D., Jr., Mejia, E., Mathews, E., Ure, K., Ogawa, S., Sinton, C.M., Gage, F.H., and Hsieh, J. (2007). Epigenetic modulation of seizure-induced neurogenesis and cognitive decline. J. Neurosci. *27*, 5967–5975.

Joint Epilepsy Council (2011). Epilepsy Prevalence, Incidence, and Other Statistic (Joint Epilepsy Council Publication).

Juliandi, B., Abematsu, M., Sanosaka, T., Tsujimura, K., Smith, A., and Nakashima, K. (2012). Induction of superficial cortical layer neurons from mouse embryonic stem cells by valproic acid. Neurosci. Res. *72*, 23–31.

Jung, G.A., Yoon, J.Y., Moon, B.S., Yang, D.H., Kim, H.Y., Lee, S.H., Bryja, V., Arenas, E., and Choi, K.Y. (2008). Valproic acid induces differentiation and inhibition of proliferation in neural progenitor

cells via the beta-catenin-Ras-ERK-p21Cip/WAF1 pathway. BMC Cell Biol. *9*, 66.

Kazantsev, A.G., and Thompson, L.M. (2008). Therapeutic application of histone deacetylase inhibitors for central nervous system disorders. Nat. Rev. Drug Discov. *7*, 854–868.

Kohman, R.A., Bhattacharya, T.K., Wojcik, E., and Rhodes, J.S. (2013). Exercise reduces activation of microglia isolated from hippocampus and brain of aged mice. J. Neuroinflammation *10*, 114.

Kostrouchová, M., Kostrouch, Z., and Kostrouchová, M. (2007). Valproic acid, a molecular lead to multiple regulatory pathways. Folia Biol. (Praha) *53*, 37–49.

LeDoux, J. (2003). The emotional brain, fear, and the amygdala. Cell. Mol. Neurobiol. *23*, 727–738.

MacDonald, J.L., and Roskams, A.J. (2008). Histone deacetylases 1 and 2 are expressed at distinct stages of neuro-glial development. Dev. Dyn. *237*, 2256–2267.

MacDonald, J.L., Gin, C.S., and Roskams, A.J. (2005). Stage-specific induction of DNA methyltransferases in olfactory receptor neuron development. Dev. Biol. *288*, 461–473.

Matsuda, T., Murao, N., Katano, Y., Juliandi, B., Kohyama, J., Akira, S., Kawai, T., and Nakashima, K. (2015). TLR9 signalling in microglia attenuates seizure-induced aberrant neurogenesis in the adult hippocampus. Nat. Commun. *6*, 6514.

Meador, K.J., Baker, G.A., Browning, N., Clayton-Smith, J., Combs-Cantrell, D.T., Cohen, M., Kalayjian, L.A., Kanner, A., Liporace, J.D., Pennell, P.B., et al.; NEAD Study Group (2009). Cognitive function at 3 years of age after fetal exposure to antiepileptic drugs. N. Engl. J. Med. *360*, 1597–1605.

Meador, K.J., Baker, G.A., Browning, N., Cohen, M.J., Clayton-Smith, J., Kalayjian, L.A., Kanner, A., Liporace, J.D., Pennell, P.B., Privitera, M., and Loring, D.W.; NEAD Study Group (2011). Foetal antiepileptic drug exposure and verbal versus non-verbal abilities at three years of age. Brain *134*, 396–404.

Meador, K.J., Baker, G.A., Browning, N., Cohen, M.J., Bromley, R.L., Clayton-Smith, J., Kalayjian, L.A., Kanner, A., Liporace, J.D., Pennell, P.B., et al.; NEAD Study Group (2012). Effects of fetal antiepileptic drug exposure: outcomes at age 4.5 years. Neurology *78*, 1207–1214.

Meador, K.J., Baker, G.A., Browning, N., Cohen, M.J., Bromley, R.L., Clayton-Smith, J., Kalayjian, L.A., Kanner, A., Liporace, J.D., Pennell, P.B., et al.; NEAD Study Group (2013). Fetal antiepileptic drug exposure and cognitive outcomes at age 6 years (NEAD study): a prospective observational study. Lancet Neurol. *12*, 244–252.

Meinardi, H., Scott, R.A., Reis, R., and Sander, J.W.; ILAE Commission on the Developing World (2001). The treatment gap in epilepsy: the current situation and ways forward. Epilepsia *42*, 136–149.

Molyneaux, B.J., Arlotta, P., Menezes, J.R., and Macklis, J.D. (2007). Neuronal subtype specification in the cerebral cortex. Nat. Rev. Neurosci. *8*, 427–437.

Murabe, M., Yamauchi, J., Fujiwara, Y., Hiroyama, M., Sanbe, A., and Tanoue, A. (2007). A novel embryotoxic estimation method of VPA using ES cells differentiation system. Biochem. Biophys. Res. Commun. *352*, 164–169.

Nau, H., Hauck, R.S., and Ehlers, K. (1991). Valproic acid-induced neural tube defects in mouse and human: aspects of chirality, alternative drug development, pharmacokinetics and possible mechanisms. Pharmacol. Toxicol. *69*, 310–321.

Ngugi, A.K., Bottomley, C., Kleinschmidt, I., Sander, J.W., and Newton, C.R. (2010). Estimation of the burden of active and lifetime epilepsy: a meta-analytic approach. Epilepsia *51*, 883–890.

Phiel, C.J., Zhang, F., Huang, E.Y., Guenther, M.G., Lazar, M.A., and Klein, P.S. (2001). Histone deacetylase is a direct target of valproic acid, a potent anticonvulsant, mood stabilizer, and teratogen. J. Biol. Chem. *276*, 36734–36741.

Rosenberg, G. (2007). The mechanisms of action of valproate in neuropsychiatric disorders: can we see the forest for the trees? Cell. Mol. Life Sci. *64*, 2090–2103.

Sander, J.W. (2003). The epidemiology of epilepsy revisited. Curr. Opin. Neurol. *16*, 165–170.

Sarnyai, Z., Sibille, E.L., Pavlides, C., Fenster, R.J., McEwen, B.S., and Tóth, M. (2000). Impaired hippocampal-dependent learning and functional abnormalities in the hippocampus in mice lacking serotonin(1A) receptors. Proc. Natl. Acad. Sci. USA *97*, 14731–14736.

Saxe, M.D., Battaglia, F., Wang, J.W., Malleret, G., David, D.J., Monckton, J.E., Garcia, A.D., Sofroniew, M.V., Kandel, E.R., Santarelli, L., et al. (2006). Ablation of hippocampal neurogenesis impairs contextual fear conditioning and synaptic plasticity in the dentate gyrus. Proc. Natl. Acad. Sci. USA *103*, 17501–17506.

Shen, S., Li, J., and Casaccia-Bonnefil, P. (2005). Histone modifications affect timing of oligodendrocyte progenitor differentiation in the developing rat brain. J. Cell Biol. *169*, 577–589.

Shors, T.J., Townsend, D.A., Zhao, M., Kozorovitskiy, Y., and Gould, E. (2002). Neurogenesis may relate to some but not all types of hippocampal-dependent learning. Hippocampus *12*, 578–584.

Sierra, A., Encinas, J.M., Deudero, J.J., Chancey, J.H., Enikolopov, G., Overstreet-Wadiche, L.S., Tsirka, S.E., and Maletic-Savatic, M. (2010). Microglia shape adult hippocampal neurogenesis through apoptosis-coupled phagocytosis. Cell Stem Cell *7*, 483–495.

Stranahan, A.M. (2011). Physiological variability in brain-derived neurotrophic factor expression predicts dendritic spine density in the mouse dentate gyrus. Neurosci. Lett. *495*, 60–62.

Suh, H., Deng, W., and Gage, F.H. (2009). Signaling in adult neurogenesis. Annu. Rev. Cell Dev. Biol. *25*, 253–275.

Sun, G., Fu, C., Shen, C., and Shi, Y. (2011). Histone deacetylases in neural stem cells and induced pluripotent stem cells. J. Biomed. Biotechnol. *2011*, 835968.

Tolwani, R.J., Buckmaster, P.S., Varma, S., Cosgaya, J.M., Wu, Y., Suri, C., and Shooter, E.M. (2002). BDNF overexpression increases dendrite complexity in hippocampal dentate gyrus. Neuroscience *114*, 795–805.

Turrigiano, G. (2011). Too many cooks? Intrinsic and synaptic homeostatic mechanisms in cortical circuit refinement. Annu. Rev. Neurosci. *34*, 89–103.

Turrigiano, G.G., and Nelson, S.B. (2004). Homeostatic plasticity in the developing nervous system. Nat. Rev. Neurosci. *5*, 97–107.

Van der Borght, K., Havekes, R., Bos, T., Eggen, B.J., and Van der Zee, E.A. (2007). Exercise improves memory acquisition and retrieval in the Y-maze task: relationship with hippocampal neurogenesis. Behav. Neurosci. *121*, 324–334.

van Praag, H. (2009). Exercise and the brain: something to chew on. Trends Neurosci. *32*, 283–290.

van Praag, H., Christie, B.R., Sejnowski, T.J., and Gage, F.H. (1999a). Running enhances neurogenesis, learning, and long-term potentiation in mice. Proc. Natl. Acad. Sci. USA *96*, 13427–13431.

van Praag, H., Kempermann, G., and Gage, F.H. (1999b). Running increases cell proliferation and neurogenesis in the adult mouse dentate gyrus. Nat. Neurosci. *2*, 266–270.

van Praag, H., Shubert, T., Zhao, C., and Gage, F.H. (2005). Exercise enhances learning and hippocampal neurogenesis in aged mice. J. Neurosci. *25*, 8680–8685.

van Strien, N.M., Cappaert, N.L., and Witter, M.P. (2009). The anatomy of memory: an interactive overview of the parahippocampal-hippocampal network. Nat. Rev. Neurosci. *10*, 272–282.

Vukovic, J., Colditz, M.J., Blackmore, D.G., Ruitenberg, M.J., and Bartlett, P.F. (2012). Microglia modulate hippocampal neural precursor activity in response to exercise and aging. J. Neurosci. *32*, 6435–6443.

Wojtowicz, J.M., Askew, M.L., and Winocur, G. (2008). The effects of running and of inhibiting adult neurogenesis on learning and memory in rats. Eur. J. Neurosci. *27*, 1494–1502.

Yang, R.J., Mozhui, K., Karlsson, R.M., Cameron, H.A., Williams, R.W., and Holmes, A. (2008). Variation in mouse basolateral amygdala volume is associated with differences in stress reactivity and fear learning. Neuropsychopharmacology *33*, 2595–2604.

Yu, I.T., Park, J.Y., Kim, S.H., Lee, J.S., Kim, Y.S., and Son, H. (2009). Valproic acid promotes neuronal differentiation by induction of proneural factors in association with H4 acetylation. Neuropharmacology *56*, 473–480.

Yuan, P.X., Huang, L.D., Jiang, Y.M., Gutkind, J.S., Manji, H.K., and Chen, G. (2001). The mood stabilizer valproic acid activates mitogen-activated protein kinases and promotes neurite growth. J. Biol. Chem. *276*, 31674–31683.

Zhao, C., Deng, W., and Gage, F.H. (2008). Mechanisms and functional implications of adult neurogenesis. Cell *132*, 645–660.

Stem Cell Reports

Supplemental Information

Reduced Adult Hippocampal Neurogenesis and Cognitive Impairments following Prenatal Treatment of the Antiepileptic Drug Valproic Acid

Berry Juliandi, Kentaro Tanemura, Katsuhide Igarashi, Takashi Tominaga, Yusuke Furukawa, Maky Otsuka, Noriko Moriyama, Daigo Ikegami, Masahiko Abematsu, Tsukasa Sanosaka, Keita Tsujimura, Minoru Narita, Jun Kanno, and Kinichi Nakashima

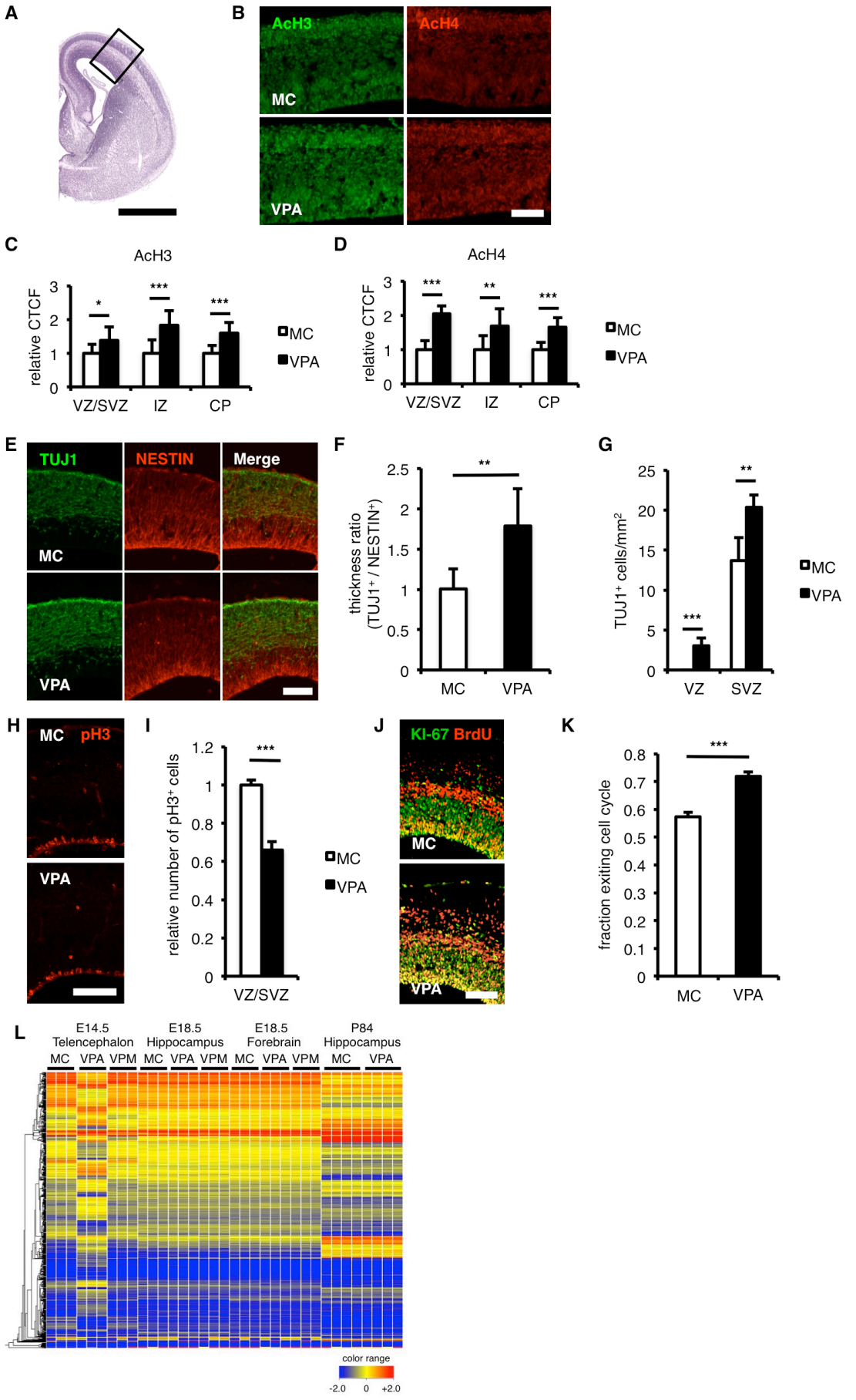
A
B
AcH3
AcH4
MC
VPA
C
AcH3
relative CTCF
VZ/SVZ
IZ
CP
MC
VPA
D
AcH4
relative CTCF
VZ/SVZ
IZ
CP
MC
VPA
E
TUJ1
NESTIN
Merge
MC
VPA
F
thickness ratio (TUJ1+ / NESTIN+)
MC
VPA
G
TUJ1+ cells/mm2
VZ
SVZ
MC
VPA
H
MC
pH3
VPA
I
relative number of pH3+ cells
VZ/SVZ
MC
VPA
J
KI-67 BrdU
MC
VPA
K
fraction exiting cell cycle
MC
VPA
L
E14.5 Telencephalon
E18.5 Hippocampus
E18.5 Forebrain
P84 Hippocampus
MC VPA VPM MC VPA VPM MC VPA VPM MC VPA
color range
-2.0 0 +2.0

Figure S1, Related to Figure 1

Prenatal VPA treatment increases histone acetylation and enhances embryonic neurogenesis

(A) E15.5 forebrain sections from the region highlighted by the black rectangle were used for analysis. The image was modified from the Electronic Prenatal Mouse Brain Atlas. (B-D) VPA increases global histone acetylation of histones H3 (AcH3; green in B; quantification in C) and H4 (AcH4; red in B; quantification in D) in the embryonic forebrain. (E and F) The thickness ratio of regions positive for the immature neuron marker β-tubulin isotype III (TUJ1; green in E) and the NPC marker NESTIN (red in E) is increases in the cortex of VPA-treated mice (F), indicating that VPA enhances neurogenesis and depletes the NPC pool in the embryonic forebrain. (G) Quantification of $TUJ1^+$ cells in the VZ and SVZ in E. (H and I) VPA treatment reduces the number of mitotic NPCs ($pH3^+$; red in H) in the VZ and SVZ (I). (J) The fraction of cells exiting the cell cycle at E15.5 is higher in VPA-treated mice, as shown by an increased number of $BrdU^+$ cells (red) that were negative for KI-67 (green), 1 day after a single BrdU injection at E14.5. (K) Quantification of $BrdU^+$ cells that were negative for KI-67 compared to $BrdU^+$ cells that were still positive for KI-67 in J. (L) Hierarchical gene clustering of gene expression level shows that VPA transiently changed global gene expression through its HDAC-inhibiting activity. Red and blue bars indicate genes expressed at relatively high and low levels (more than 2.0-fold), respectively, in each stage and condition (n = 3 for each group at E14.5 and E18.5; n = 4 for each group at P84). See Gene Expression Omnibus (http://www.ncbi.nlm.nih.gov/geo), accession number GSE 42904, for complete data sets. MC, prenatal methylcellulose (vehicle); VPA, prenatal valproic acid; VPM, prenatal valpromide; VZ, ventricular zone; SVZ, subventricular zone; IZ,

intermediate zone; CP, cortical plate; CTCF, corrected total cell fluorescence. Data are represented as means. n = 3 for each group. Error bars are SD. *$P < 0.05$, **$P < 0.01$, ***$P < 0.001$, two-tailed t-test. Scale bar is 1 mm in A, and 100 μm in B, E, H and J.

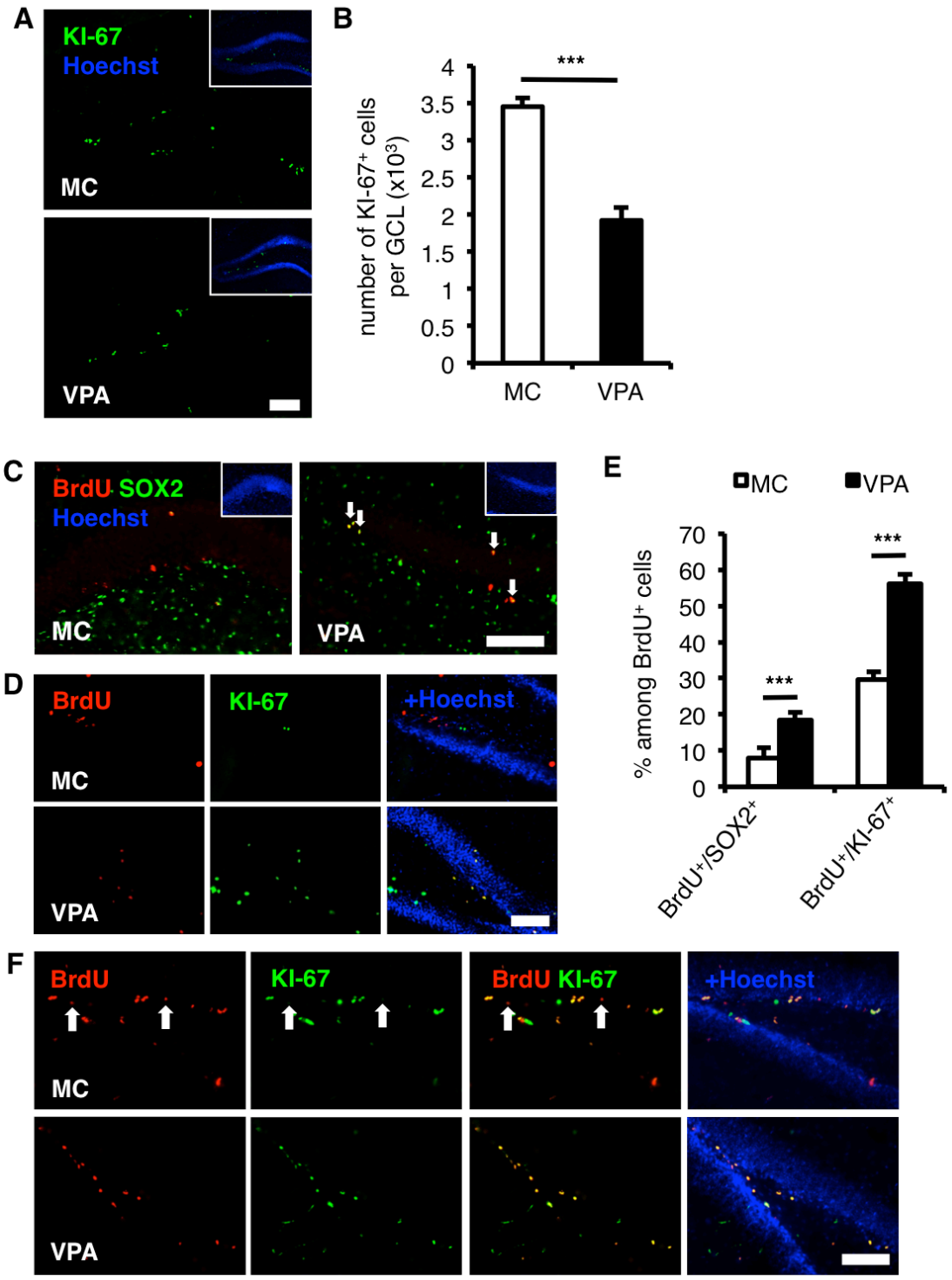

Figure S2, Related to Figure 3

VPA-treated mice have fewer proliferating cells in the DG of the hippocampus which differentiate more slowly than those in MC-treated mice

(A) Representative images of brain sections containing the DG and stained for KI-67

(green) and with Hoechst (blue) showed a reduction of proliferating cells in VPA-treated mice. (B) Quantification of KI-67^{+} cells in the granule cell layer (GCL). (C) Four weeks after the last BrdU injection, a higher proportion of BrdU-retaining cells (red) in VPA-treated mice (white arrows) still expressed the NPC marker SOX2 (green). (D) Four weeks after the last BrdU injection, a higher proportion of BrdU-retaining cells (red) in VPA-treated mice still expressed the proliferation marker KI-67 (green). (E) Quantification of BrdU^{+}SOX2^{+} and BrdU^{+}KI-67^{+} cells at 4 weeks after the last BrdU injection. (F) One day after the last BrdU injection, almost all BrdU^{+} cells (red) were still KI-67^{+} (green) in VPA-treated mice, while several BrdU^{+} but KI-67^{-} cells already existed in MC-treated mice (white arrows). MC, prenatal methylcellulose (vehicle); VPA, prenatal valproic acid. Data are represented as means. n = 3 for each group. Error bars are SD. ***$P < 0.001$, two-tailed t-test. Scale bars are 100 μm. See Figure 3A for experimental timeline.

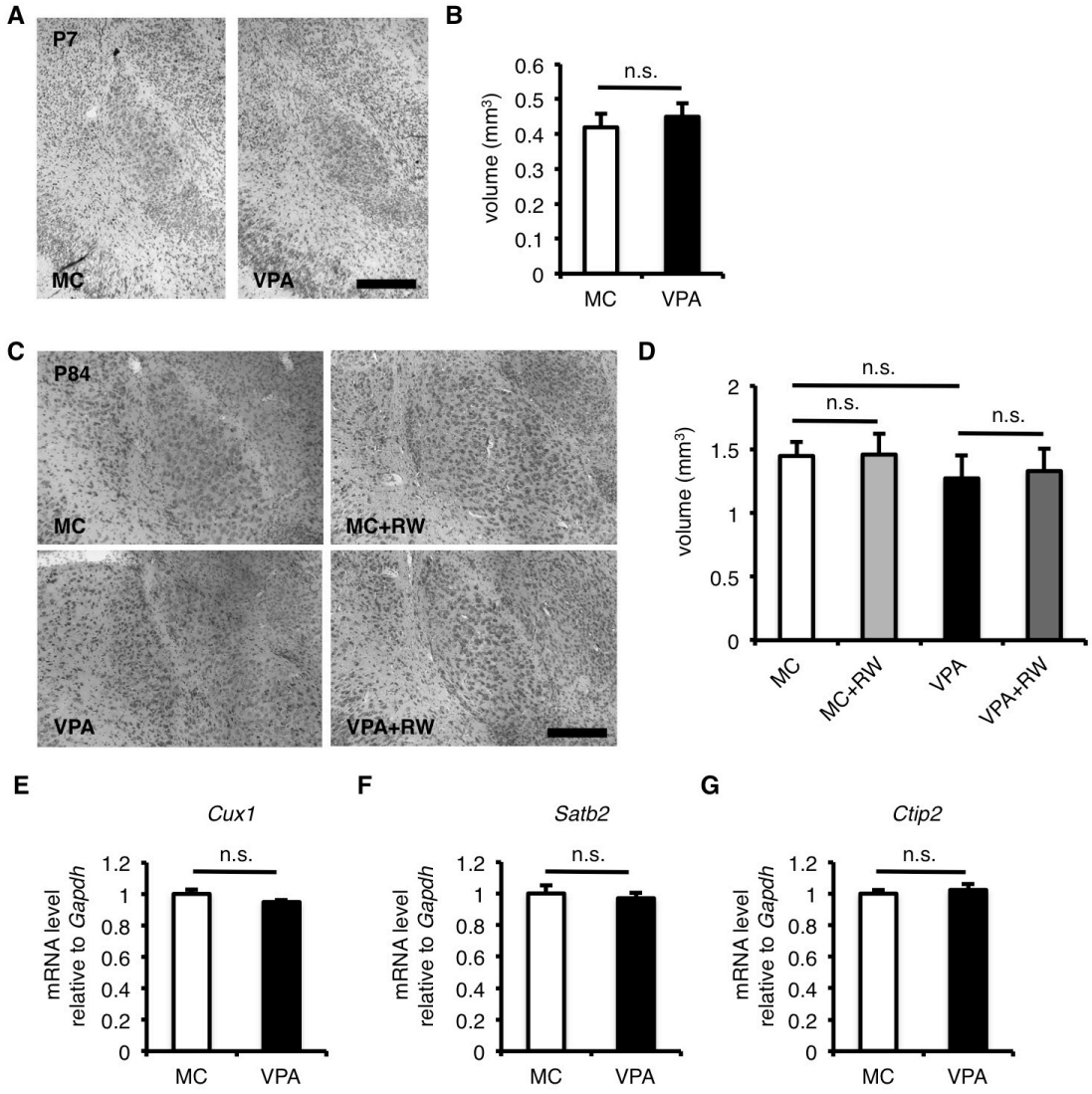

Figure S3, Related to Figure 3

The size of amygdala and expression levels of cortical-layer genes are not altered

(A-D) Representative images of brain sections containing amygdala stained with thionin (A and C), and the measurement of amygdala volume (B and D) showed no significant difference between MC- and VPA-treated mice. Postnatal voluntary running did not influence the amygdala size in both MC- and VPA-treated mice (D). (E-G) The expression levels of superficial-layer (*cut-like homeobox 1*, *Cux1*; E and *special AT-rich sequence binding protein 2*, *Satb2*; F), and deep-layer neuronal genes (*B-cell leukemia/lymphoma 11B*, *Bcl11b* also called *Ctip2*; G) are similar between MC- and VPA-treated mice in P84 cerebral cortex. MC, prenatal methylcellulose

(vehicle); MC+RW, prenatal methylcellulose and postnatal running; VPA, prenatal valproic acid; VPA+RW, prenatal valproic acid and postnatal running; *Gapdh, glyceraldehyde 3-phosphate dehydrogenase*. Data are represented as means. n = 3 for each group. Error bars are SD. n.s., not significantly different, two-tailed t-test. Scale bars are 250 μm.

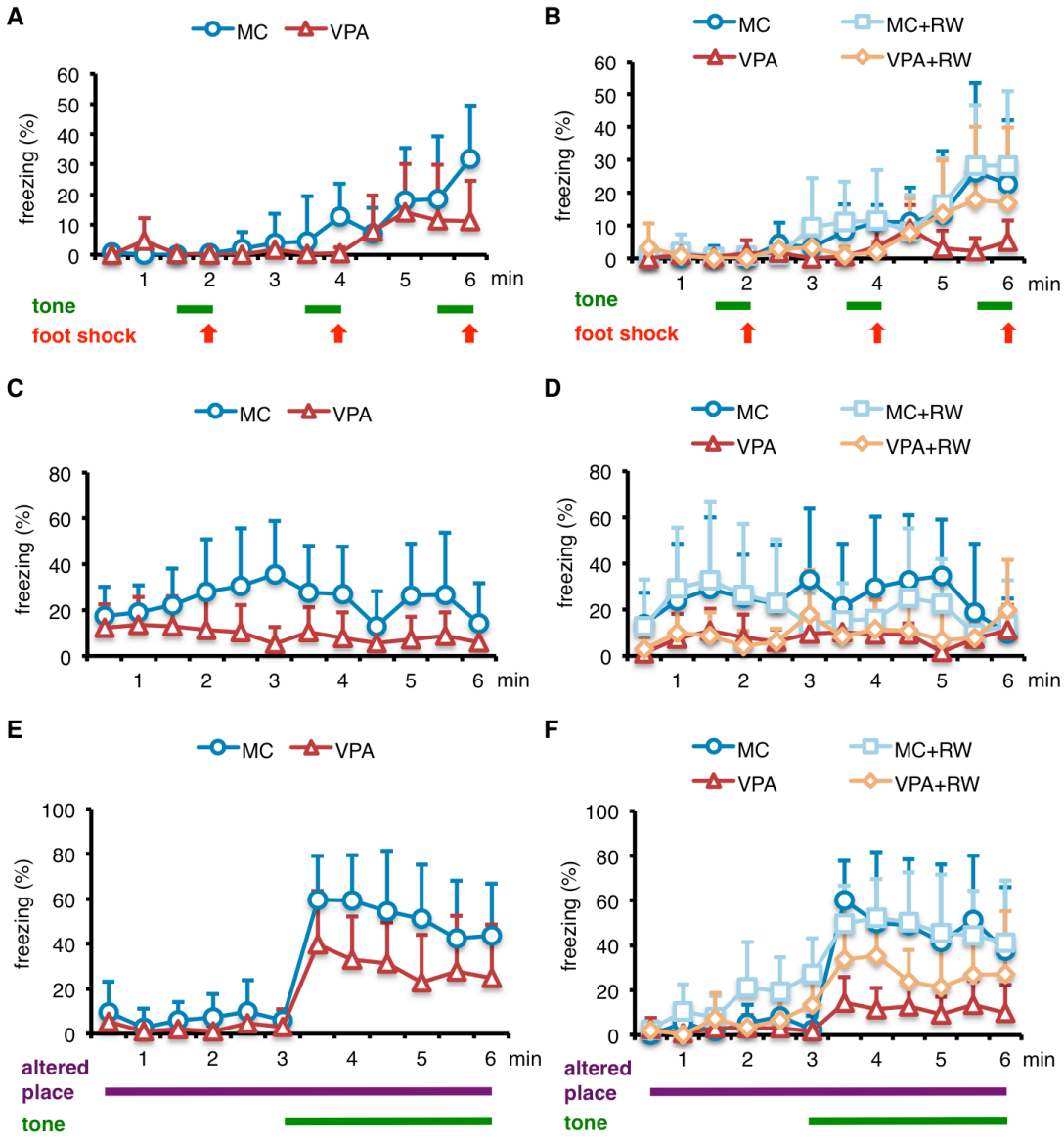

Figure S4, Related to Figure 2

Time course of freezing response in associative learning and memory tests

(A) VPA-treated mice (n = 12) displayed a lower freezing response than MC-treated mice (control; n = 12) in conditioned fear tests (day 1). (B) Voluntary running reinstates the freezing response in conditioned fear tests of VPA-treated mice (day 1; n = 7 for MC and VPA+RW; n = 8 for MC+RW and VPA). (C) VPA-treated mice (n = 12) displayed a lower freezing response than MC-treated mice (control; n = 12) in contextual fear tests (day 2). (D) Voluntary running does not reinstate the freezing

response in contextual fear tests of VPA-treated mice (day 2; n = 7 for MC and VPA+RW; n = 8 for MC+RW and VPA). (E) VPA-treated mice (n = 12) displayed a lower freezing response than MC-treated mice (control; n = 12) in cued fear tests (day 3). (F) Voluntary running reinstates the freezing response in cued fear tests of VPA-treated mice (day 3; n = 7 for MC and VPA+RW; n = 8 for MC+RW and VPA). MC, prenatal methylcellulose (vehicle); MC+RW, prenatal methylcellulose and postnatal running; VPA, prenatal valproic acid; VPA+RW, prenatal valproic acid and postnatal running. Data are represented as means. Error bars are SD.

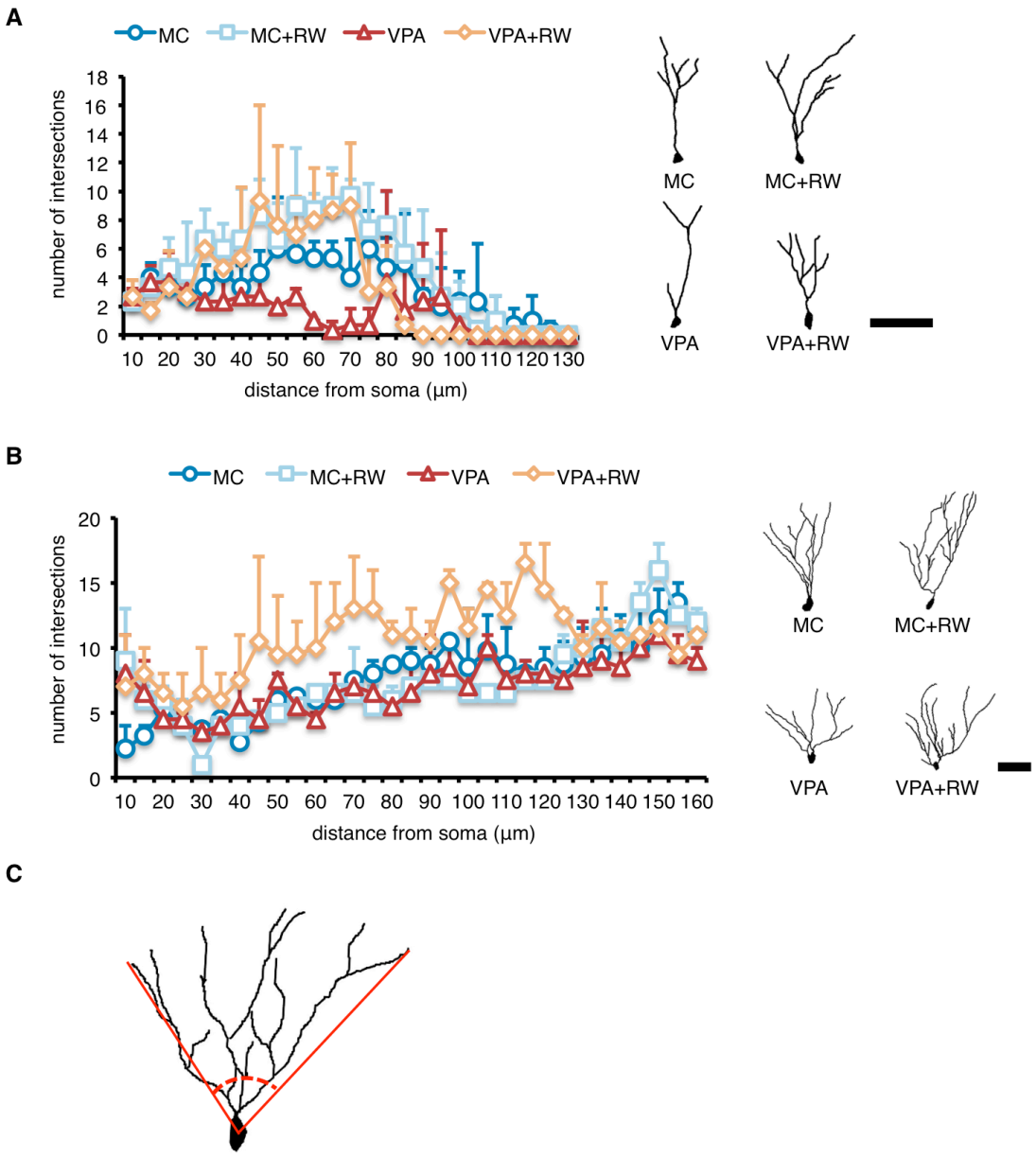

Figure S5, Related to Figure 5

Morphometry of DG neurons

(A) Sholl analysis showed that DCX^+ immature neurons in VPA-treated mice have a lower dendritic complexity than MC-treated mice, and voluntary running increases dendritic complexity in both MC- and VPA-treated mice. (B) Sholl analysis showed that Golgi-Cox stained neurons in VPA-treated mice have a similar dendritic complexity to MC-treated mice, and voluntary running increases dendritic complexity

in VPA-treated mice. The diagrams on the right in (A) and (B) shows representative neurons for each treatments. (C) Graphical example of maximal dendritic span measurement used for Figures 5G-5I. The solid red line represents the maximal dendritic span and dashed red line represents the angle that was used for analysis. MC, prenatal methylcellulose (vehicle); MC+RW, prenatal methylcellulose and postnatal running; VPA, prenatal valproic acid; VPA+RW, prenatal valproic acid and postnatal running. Data are represented as means. n = 3 for each group. Error bars are SD. Scale bar is 50 μm in A, and 100 μm in B.

Table S1, Related to Figure 2

Summary of behavior test results on 12-13-week-old male mice

Behavior Test	MC[a]	VPA[a]
Open Field		
- total distance (cm)	3648.30 ± 513.55	2436.49 ± 407.28*
- total center (sec)	94.33 ± 37.38	77.83 ± 48.24
- average speed (cm/sec)	4.79 ± 0.85	4.06 ± 0.67
- moving speed (cm/sec)	8.92 ± 0.66	8.10 ± 0.49
- move episode (times)	187.17 ± 11.37	184.17 ± 11.77
- total movement (times)	320.04 ± 40.39	299.71 ± 39.02
- distance per movement (cm)	15.33 ± 2.63	13.21 ± 1.93*
- duration per movement (sec)	1.72 ± 0.20	1.62 ± 0.17
Light/Dark Transition		
- dark distance (cm)	830.88 ± 122.36	639.25 ± 66.66***
- light distance (cm)	312.03 ± 127.66	237.76 ± 120.83
- dark time (sec)	227.92 ± 29.47	224.33 ± 31.14
- light time (sec)	85.21 ± 31.02	84.75 ± 30.13
- number of transitions (times)	14.00 ± 5.70	8.42 ± 4.58*
- latency to enter light (sec)	83.33 ± 68.79	98.00 ± 48.26
Elevated Plus Maze		
- total distance (cm)	1591.45 ± 263.67	1372.97 ± 235.90*
- open arms time (sec)	181.46 ± 56.73	196.00 ± 46.52
- closed arms time (sec)	418.54 ± 56.73	404.00 ± 46.52
- open arms entry (times)	4.75 ± 3.47	5.42 ± 3.37
- closed arms entry (times)	28.33 ± 7.28	21.83 ± 4.28*
- total entry (times)	33.08 ± 8.27	27.25 ± 6.40
Y-Maze		
- total distance (cm)	1365.93 ± 228.01	1095.63 ± 154.07**
- total entry (times)	16.92 ± 3.15	12.66 ± 2.42***
- alternation rate (% correct)	66.15 ± 13.01	50.51 ± 21.18*
Fear Conditioning		
- conditioning (% freezing)	8.31 ± 5.81	4.40 ± 4.10*
- contextual (% freezing)	23.97 ± 12.79	9.32 ± 5.39**
- cued (% freezing)	51.81 ± 18.46	29.91 ± 18.03**
- moving speed without foot shock (cm/sec)	0.90 ± 0.40	1.00 ± 0.40
- moving speed with foot shock (cm/sec)	11.40 ± 3.10	8.10 ± 2.60
Prepulse Inhibition		
- 80/120 dB (% startle)	31.55 ± 23.59	12.21 ± 26.83
- 85/120 dB (% startle)	28.82 ± 22.73	24.15 ± 22.03
- 90/120 dB (% startle)	38.82 ± 20.95	34.35 ± 21.94
- 95/120 dB (% startle)	57.35 ± 17.32	41.02 ± 19.23*
- 100/120 dB (% startle)	74.71 ± 12.16	65.66 ± 18.38
- 105/120 dB (% startle)	90.88 ± 3.90	83.24 ± 11.66

Tail Suspension (% immobility)	53.61 ± 26.07	54.53 ± 26.82
Thermal Hyperalgesia		
- left paw withdrawal latency (sec)	9.37 ± 1.24	9.37 ± 2.04
- right paw withdrawal latency (sec)	8.70 ± 1.71	9.37 ± 2.02
Tactile Allodynia		
- left paw, 0.02g (allodynia score)	0.08 ± 0.31	0.25 ± 0.26
- right paw, 0.02g (allodynia score)	0.17 ± 0.33	0.08 ± 0.19
- left paw, 0.16g (allodynia score)	0.33 ± 0.33	0.08 ± 0.23
- right paw, 0.16g (allodynia score)	0.08 ± 0.23	0.08 ± 0.23

[a] n = 12 mice.

*$P < 0.05$, **$P < 0.01$, ***$P < 0.001$, two-tailed t-test.

MC, prenatal methylcellulose (vehicle); VPA, prenatal valproic acid.

Table S2, Related to Figure 4

Summary of behavior test results and two-way ANOVA analysis with or without postnatal running on 12-13-week-old male mice

Behavior Test	MC[a]	MC+RW[b]	VPA[b]	VPA+RW[a]	Two-way ANOVA factors		
					Prenatal treatment	Postnatal activity	Interaction
Open Field							
- total distance (cm)	2910.14 ± 195.27	2843.67 ± 674.96	2634.54 ± 447.83	2884.70 ± 519.33	$F(1, 26) = 0.46$, $p = 0.50$	$F(1, 26) = 0.25$, $p = 0.62$	$F(1, 26) = 0.75$, $p = 0.39$
- total center (sec)	162.57 ± 77.93	223.31 ± 87.23	151.00 ± 97.77	183.36 ± 65.68	$F(1, 26) = 0.89$, $p = 0.35$	$F(1, 26) = 2.30$, $p = 0.14$	$F(1, 26) = 0.21$, $p = 0.65$
- average speed (cm/sec)	4.84 ± 0.32	4.74 ± 1.12	4.39 ± 0.75	4.80 ± 0.86	$F(1, 26) = 0.47$, $p = 0.50$	$F(1, 26) = 0.26$, $p = 0.62$	$F(1, 26) = 0.73$, $p = 0.40$
- moving speed (cm/sec)	8.96 ± 0.41	9.73 ± 0.91	8.12 ± 0.57	9.43 ± 0.80	$F(1, 26) = 6.03$, $p < 0.05$	$F(1, 26) = 16.07$, $p < 0.001$	$F(1, 26) = 1.07$, $p = 0.31$
- move episode (times)	196.71 ± 12.22	173.50 ± 21.23	180.75 ± 13.36	178.43 ± 10.33	$F(1, 26) = 0.71$, $p = 0.41$	$F(1, 26) = 5.33$, $p < 0.05$	$F(1, 26) = 3.56$, $p = 0.07$
- total movement (times)	324.36 ± 16.72	291.94 ± 55.80	323.62 ± 38.70	305.07 ± 41.72	$F(1, 26) = 0.27$, $p = 0.61$	$F(1, 26) = 2.84$, $p = 0.10$	$F(1, 26) = 0.21$, $p = 0.65$
- distance per movement (cm)	14.81 ± 1.16	16.41 ± 3.30	14.56 ± 2.05	16.10 ± 2.20	$F(1, 26) = 0.20$, $p = 0.66$	$F(1, 26) = 3.34$, $p = 0.08$	$F(1, 26) = 0.001$, $p = 0.97$
- duration per movement (sec)	1.65 ± 0.08	1.69 ± 0.21	1.79 ± 0.15	1.71 ± 0.17	$F(1, 26) = 1.83$, $p = 0.19$	$F(1, 26) = 0.13$, $p = 0.72$	$F(1, 26) = 0.76$, $p = 0.39$
Light/Dark Transition							
- dark distance (cm)	857.43 ± 53.37	820.00 ± 216.94	672.85 ± 122.91**	682.67 ± 148.20**	$F(1, 26) = 8.55$, $p < 0.01$	$F(1, 26) = 0.06$, $p = 0.80$	$F(1, 26) = 0.19$, $p = 0.67$
- light distance (cm)	353.29 ±	294.43 ±	339.70 ±	288.81 ±	$F(1, 26) = 0.01$,	$F(1, 26) = 1.21$,	$F(1, 26) = 0.01$,

	117.37	117.09	173.78	124.93	$p = 0.91$	$p = 0.28$	$p = 0.91$
- dark time (sec)	211.29 ± 24.58	235.31 ± 27.17	203.75 ± 51.36	224.07 ± 41.45	$F(1, 26) = 0.61$, $p = 0.44$	$F(1, 26) = 2.54$, $p = 0.12$	$F(1, 26) = 0.02$, $p = 0.89$
- light time (sec)	101.36 ± 26.82	76.12 ± 27.86	111.06 ± 53.21	86.00 ± 44.39	$F(1, 26) = 0.62$, $p = 0.44$	$F(1, 26) = 2.96$, $p = 0.10$	$F(1, 26) = 0.001$, $p = 0.99$
- number of transitions (times)	13.29 ± 4.39	14.62 ± 7.03	11.37 ± 5.63	12.14 ± 5.90	$F(1, 26) = 1.12$, $p = 0.30$	$F(1, 26) = 0.24$, $p = 0.63$	$F(1, 26) = 0.02$, $p = 0.89$
- latency to enter light (sec)	37.14 ± 14.46	77.75 ± 58.32	119.00 ± 197.46	76.71 ± 96.32	$F(1, 26) = 0.90$, $p = 0.35$	$F(1, 26) = 0.001$, $p = 0.99$	$F(1, 26) = 0.94$, $p = 0.34$
Y-Maze							
- total distance (cm)	733.94 ± 217.46	681.06 ± 298.66	595.24 ± 350.61	578.36 ± 176.34	$F(1, 26) = 1.40$, $p = 0.25$	$F(1, 26) = 0.12$, $p = 0.73$	$F(1, 26) = 0.03$, $p = 0.86$
- total entry (times)	9.29 ± 2.98	8.50 ± 3.46	7.12 ± 4.05	7.14 ± 1.57	$F(1, 26) = 2.19$, $p = 0.15$	$F(1, 26) = 0.11$, $p = 0.75$	$F(1, 26) = 0.12$, $p = 0.73$
- alternation rate (% correct)	59.66 ± 20.13	69.96 ± 16.78	26.37 ± 18.94**	66.86 ± 12.82	$F(1, 26) = 9.76$, $p < 0.01$	$F(1, 26) = 15.85$, $p < 0.001$	$F(1, 26) = 5.59$, $p < 0.05$
Fear Conditioning							
- conditioning (% freezing)	8.51 ± 6.83	9.84 ± 7.33	2.38 ± 1.73*	5.80 ± 5.23	$F(1, 26) = 6.38$, $p < 0.05$	$F(1, 26) = 1.30$, $p = 0.26$	$F(1, 26) = 0.25$, $p = 0.62$
- contextual (% freezing)	24.54 ± 20.61	20.00 ± 13.96	7.71 ± 4.39**	9.62 ± 6.37**	$F(1, 26) = 8.30$, $p < 0.01$	$F(1, 26) = 0.08$, $p = 0.78$	$F(1, 26) = 0.47$, $p = 0.50$
- cued (% freezing)	48.25 ± 26.13	47.22 ± 16.02	11.95 ± 5.06**	28.09 ± 16.74	$F(1, 26) = 20.03$, $p < 0.001$	$F(1, 26) = 1.43$, $p = 0.24$	$F(1, 26) = 1.85$, $p = 0.19$

[a] n = 7 mice.

[b] n = 8 mice.

*$P < 0.05$, **$P < 0.01$, two-tailed t-test to MC.

MC, prenatal methylcellulose (vehicle); MC+RW, prenatal methylcellulose and postnatal running; VPA, prenatal valproic acid; VPA+RW, prenatal valproic acid and postnatal running.

Supplemental Experimental Procedures

Animal Group and Treatment. Mice were randomly assigned to each group on embryonic day (E)6.5. The VPA and VPM groups received an oral administration of 300 mg/kg valproic acid (VPA; Sigma) and valpromide (VPM; Wako), respectively, once a day on E12.5, E13.5, and E14.5. The MC group received an oral administration of identical volumes of 0.5% (w/v) MC (Wako) once a day on the same days. Pups from the MC and VPA groups were weaned at postnatal day (P)28 and 4 male mice per litter were randomly selected and housed in one cage. Four groups were designated as MC (pups from an MC-treated mother), MC+RW (pups from an MC-treated mother, with running wheel), VPA (pups from a VPA-treated mother), and VPA+RW (pups from a VPA-treated mother, with RW). MC+RW and VPA+RW mice were housed with a RW (Fast-Trac, BioServ) and were allowed to run freely in their cage immediately after weaning. To analyze adult neurogenesis, 100 mg/kg BrdU was injected intraperitoneally for 7 consecutive days starting on P84. Mice were sacrificed one day (proliferation group) or 4 weeks (differentiation group) after the last BrdU injection. For behavioral and electrophysiological analysis, separate sets of 12-13-week-old male mice with the same group designations were used.

Immunohistochemistry. Mice were anesthesized and perfused with PBS followed by 4% PFA in PBS on the indicated days. The brain was dissected, and postfixed overnight in the same fixative at 4 °C. For cryosectioning, fixed tissues were cryoproctected in 10% sucrose in PBS overnight at 4 °C, then in 20% sucrose in PBS overnight at 4 °C, and embedded in OCT compound (Tissue Tek). Cryostat sections

(15 μm) of embryonic and P7 brains were cut and affixed to MAS-coated glass slides (Matsunami Glass), while other postnatal brain sections (40 μm) were cut and suspended in PBS in 6- or 12-well plates (Nunc, Greiner). For some antibodies, antigen retrieval was conducted either by incubation in L.A.B. Solution (Polysciences) for 15 min at room temperature (RT) or by autoclaving in Target Retrieval Solution (Dako) for 15 min at 105 °C. For BrdU immunostaining, sections were incubated with 2 N HCl for 30 min at 37 °C. After 3 washes with PBS, the sections were incubated for 1 h at RT in blocking solution (PBS containing 3% FBS and 0.1% Triton X-100). They were then incubated overnight at 4 °C with the appropriate primary antibodies. The following primary antibodies were used: rabbit anti-acetyl-histone H3 (1:1000, Millipore 06-599), rabbit anti-acetyl-histone H4 (1:1000, Millipore 06-866), rabbit anti-β-tubulin isotype III (TUJ1; 1:1000, Covance PRB-435P), mouse anti-NESTIN (1:250, Millipore MAB353), goat anti-doublecortin (DCX; 1:500, Santa Cruz sc-8066), rabbit anti-doublecortin (DCX; 1:1000, Abcam ab18723), mouse anti-human KI-67 (1:500, BD Pharmingen 550609), rat anti-BrdU (1:1000, AbD Serotec OBT0030), mouse anti-phospho-histone H3 (pH3; 1:1000, Cell Signaling 9706), mouse anti-NEUN (1:100, Millipore MAB377), rabbit anti-S100β (1:500, Swant 37A), rabbit anti-SOX2 (1:500, Millipore AB5603), rabbit anti-TBR2 (1:500, Abcam ab23345), rabbit anti-IBA1 (1:500, Wako 019-19741), and rat anti-mouse CD68 (1:500, AbD Serotec MCA1957GA). After 3 washes with PBS, the sections were incubated for 2 h at RT with the appropriate secondary antibodies. The following secondary antibodies were used: Cy3-conjugated donkey anti-rabbit, Cy3-conjugated donkey anti-mouse, Cy3-conjugated donkey anti-goat, Cy3-conjugated donkey anti-rat, Cy5-conjugated donkey anti-rabbit, Cy5-conjugated donkey anti-mouse (all 1:500, Jackson ImmunoResearch), Alexa Fluor 488-conjugated donkey

anti-mouse, and Alexa Fluor 488-conjugated donkey anti-rabbit (both 1:500, Invitrogen). After 3 washes with PBS, nuclei were stained for 15 min at RT with Hoechst 33258 (Nacalai Tesque). For floating postnatal sections, after being washed with PBS, sections were affixed to MAS-coated glass slides (Matsunami Glass). Sections were mounted on cover slips with Immu-Mount (Thermo Scientific), and examined and photographed using an Axiovert 200M fluorescence microscope (Zeiss), an AF6000 fluorescence microscope (Leica), or an LSM 710 confocal microscope (Zeiss), equipped with a camera and appropriate epifluorescence filters. Cell fluorescence was measured using ImageJ (http://rsbweb.nih.gov/ij), and corrected total cell fluorescence (CTCF) was calculated as described previously (Burgess et al., 2010; Gavet and Pines, 2010). Ten cells per area were picked randomly in a section and 3 mice from each group were used for analysis.

Cell counts and volume measurements. Cell counting within the indicated areas was conducted manually using an Axiovert 200M fluorescence microscope (Zeiss), an AF6000 fluorescence microscope (Leica), or an LSM 710 confocal microscope (Zeiss) equipped with a camera and appropriate epifluorescence filters. For BrdU counting in the adult neurogenesis experiment, the total number of BrdU-positive cells was counted in every sixth section (240 μm apart). BrdU-positive cells were counted throughout the rostro-caudal extent of the granule cell layer (GCL), and the derived numbers were multiplied by 6 (slice series) to obtain total cell number per GCL. For BrdU-double (or -triple) immunostaining with other markers, every twelfth section (480 μm apart) from the proliferation and differentiation groups was used and double (or triple) labeling was confirmed in three-dimensional reconstructions of z-series. From each mouse, 50 BrdU-positive cells dispersed throughout the GCL were

picked randomly and analyzed for double (or triple) immunoreactivity. Volume measurements of amygdala were done on basolateral amygdala (BLA) complex (the portion between the external capsule and the amygdalar capsule), which includes the lateral and basolateral nuclei. Area of BLA complex was manually traced by ImageJ (http://rsbweb.nih.gov/ij) in every twelfth section. Volume was estimated by multiplying the derived number with the interval thickness between serial sections (180 μm for P7, 480 μm for P84).

Gene expression analysis. These procedures were conducted according to the Percellome method (Kanno et al., 2006) to normalize mRNA expression values to sample cell numbers by adding external spike mRNAs to the sample in proportion to the genomic DNA concentration and utilizing the spike RNA quantity data as a dose-response standard curve for each sample. Brain samples were prepared from E14.5 (3 h after the final oral administration of the drugs), E18.5, and 12-week-old (P84) mice. Samples were homogenized and lysed in 500 ml of RLT buffer (QIAGEN). Two separate 10-μl aliquots were treated with DNAse-free RNase A (Nippon Gene) in a 1.5-ml tube for 30 min at 37 °C, followed by proteinase K (Roche) for 3 h at 55 °C, and then transferred to a 96-well black plate. PicoGreen fluorescent dye (Molecular Probes) was added to each well, and the plates were incubated for 2 min at 30 °C. The DNA concentration was measured using a 96-well fluorescence plate reader with excitation at 485 nm and emission at 538 nm. Lambda phage DNA (PicoGreen kit, Molecular Probes) was used as standard. The appropriate amount of spike RNA cocktail was added to the sample homogenates in proportion to their DNA concentration. Five independent *Bacillus subtilis* poly-A RNAs were included in the grade-dosed spike cocktail. Total RNAs were purified using an RNeasy Mini kit

(QIAGEN), according to the manufacturer's instructions. First-strand cDNAs were synthesized by incubating 5 μg of total RNA with 200 U SuperScript II reverse transcriptase (Invitrogen) and 100 pmol T7-$(dT)_{24}$ primer [5'-GGCCAGTGAATTGTAATACGACTCACTATAGGGAGGCGG-$(dT)_{24}$-3']. After second-strand synthesis, the double-stranded cDNAs were purified using a GeneChip Sample Cleanup Module (Affymetrix), according to the manufacturer's instructions, and labeled by *in vitro* transcription using a BioArray HighYield RNA transcript labeling kit (Enzo Life Sciences). The labeled cRNA was again purified using a GeneChip Sample Cleanup Module and treated with fragmentation buffer at 94 °C for 35 min. For hybridization to a GeneChip Mouse Genome 430 2.0 Array (Affymetrix), 15 μg of fragmented cRNA probe was incubated with 50 pM control oligonucleotide B2, 1x eukaryotic hybridization control (1.5 pM BioB, 5 pM BioC, 25 pM BioD and 100 pM Cre), 0.1 mg/ml herring sperm DNA, 0.5 mg/ml acetylated BSA and 1x manufacturer-recommended hybridization buffer in a 45 °C rotisserie oven for 16 h. Washing and staining were performed in a GeneChip Fluidics Station (Affymetrix) using the appropriate antibody amplification, washing and staining protocols. The phycoerythrin-stained arrays were scanned as digital image files, which were analyzed with GeneChip Operating Software (Affymetrix). The expression data were converted to copy numbers of mRNA per cell by the Percellome method, quality controlled, and analyzed using Percellome software (Kanno et al., 2006) and GeneSpring (Agilent Technologies). The GeneChip data have been deposited in the NCBI Gene Expression Omnibus (GEO; http://www.ncbi.nlm.nih.gov/geo/) and are accessible through GEO series accession number GSE 42904.

For real-time qPCR, total RNAs were isolated from P84 cortex and hippocampus using Sepasol-RNA I Super G (Nacalai Tesque), and treated with DNase I (Promega).

cDNAs were synthesized from 1 μg total RNA with SuperScript VILO cDNA Synthesis Kit (Invitrogen) as recommended by the manufacturer. qRT-PCR was performed by MX3000p (Agilent Technologies) or StepOnePlus (Applied Biosystems) using KAPA SYBR FAST qPCR Master Mix Universal kit with ROX as a reference dye (KAPA Biosystems). The expression of target genes was normalized to that of glyceraldehyde 3-phosphate dehydrogenase (*Gapdh*). The gene-specific primers were as follows (5′-3′): *Cux1*: Cux1-S, TGATGGATATGAAGCGGATG; Cux1-AS, TCAGCTGGTGTTGTGGCTG; *Satb2*: Satb2-S, GGAGAATCTCTGCACCATC; Satb2-AS, GAGCTCTCCTTAGTTGGCTG; *Ctip2*: Ctip2-S, CCCGACCCTGATCTACTCAC; Ctip2-AS, TTCTCCTGCTTGGGACAGATG; *Bdnf*: Bdnf-S, CAGGAGTACATAACGGCCACC; Bdnf-AS, GTAGGCCAAGTTGCCTTGTCCGT; and *Gapdh*: Gapdh-S, ACCACAGTCCATGCC ATCAC; Gapdh-AS, TCCACCACCCTGTTGCTGTA.

Behavioral tests. Experimental apparatus and image analyzing software (Image OF4, Image LD2, Image EP2, Image FZ2, SR-9040, Image TS2 and Time YM2) were obtained from O'Hara & Co. Image OF4, Image LD2, Image EP2, Image FZ2, and Image TS2 were developed from the public domain software ImageJ. All experiments were performed sequentially using the same set of male mice and were conducted between 13:30 and 16:30. The level of background noise during behavioral testing was about 50 dB. After each trial, the apparatus was wiped clean.

Open field test. Locomotor activity was measured for 10 min using an open field apparatus made of white plastic (50 x 50 x 40 (H) cm). An LED light system was positioned 50 cm above the center of the field (50 lux at the center of the field). Total

distance travelled (cm), time spent in the central area (30% of the field) (sec), and frequency of movement were measured by Image OF4 (Tanemura et al., 2002).

Light/dark transition test. The apparatus used for the light/dark transition test consisted of a cage (21 x 42 x 25 (H) cm) divided into two chambers by a partition with an opening. One chamber was brightly illuminated (250 lux), whereas the other chamber was dark (2 lux). A mouse was placed in the dark area and allowed to move freely between the two chambers through the opening for 5 min. The latency for the first move into the light area, the total number of transitions and the time spent on each side were measured by Image LD2.

Elevated plus maze test. The plus-shaped apparatus consisted of four arms (25 x 5 cm) connected to a central square area (5 x 5 cm). Two opposed arms were enclosed with 20-cm high transparent walls and the other two were left open. The floor of the maze was made of white plastic and was elevated 60 cm above the room floor (200 lux at the center of the apparatus). A mouse was placed in the central square area of the maze, facing one of the arms, and its behavior was recorded for 10 min: the total distance traveled (cm), total time spent in open arms and the central square area (sec), and total number of entries into any of the arms were measured by Image EP2 (Tanemura et al., 2002).

Contextual/cued fear conditioning test. The apparatus consisted of a conditioning chamber (or a test chamber) (17 x 10 x 10 (H) cm) made of clear plastic with a ceiling and placed in a soundproof box. The chamber floor had stainless steel rods (2-mm diameter) spaced 5 mm apart for electric foot shock to the mouse. The soundproof box was made of white-colored wood, and was equipped with an audio speaker and light source (35 lux at the center of the floor). A CCD camera was positioned 20 cm above the ceiling of the chamber. During the conditioning trial (Day 1), mice were

placed individually in the conditioning chamber in the soundproof box and, after 90 sec, they were given three tone-shock pairings (30 sec of tone, 75 dB, 10 KHz followed by 3 sec of 0.1-mA electric shock at the end of the tone) separated by 90 sec. They were then returned to their home cage. The next day (Day 2), as a contextual fear test, they were returned to the conditioning chamber for 6 min without tone or shock. On the third day (Day 3), they were placed in a novel chamber, of different make and lacking stainless steel rods, which was situated in the soundproof box and, after 3 min, the conditioning tone only (no shock) was presented for 3 min (35 lux at the center of the floor). The freezing response of the mice was measured by Image FZ2 as a consecutive 2-sec period of immobility. Freezing rate (%) was calculated as [time freezing/session time] x 100 as described previously (Tatebayashi et al., 2002).

Prepulse inhibition test. Startle responses and prepulse inhibition (PPI) of startle responses were measured using an automatic startle reflex measurement system (SR-9040; O'Hara & Co.). A test session was started by placing a mouse in a Plexiglas cylinder, where it was left undisturbed for 10 min. The duration of white noise that was used as the startle stimulus was 40 msec for all trial types. The startle response was recorded by accelerometer for 140 msec (measuring the response every 1 msec) starting with the onset of the prepulse stimulus. The background noise level in each chamber was 70 dB. The peak startle amplitude recorded during the 140-msec sampling window was used as the dependent variable. A test session consisted of 6 trial types (two types for startle stimulus-only trials, and four types for prepulse inhibition trials). The intensity of the startle stimulus was 120 dB. The prepulse sound was presented 100 msec before the startle stimulus, and its intensity was either 80, 85, 90, 95, 100 or 105 dB. Six combinations of prepulse and startle stimuli were employed (80-120, 85-120, 90-120, 95-120, 100-120 and 105-120 dB). Six blocks of

the 6 trial types were presented in pseudorandom order such that each trial type was presented once within a block. The average inter-trial interval was 15 sec (range: 10-20 sec).

Tail suspension test. Mice were suspended 60 cm above the floor for 3 min by holding their tail. The immobility time during this period was scored. Immobility was defined as the absence of all movement except for those required for respiration, and was measured by Image TS2.

Y-maze alternation test. Exploratory activity was measured using a Y-maze apparatus made of clear plastic. The maze had 3 identical arms (40 x 9 x 16 (H) cm) at 120° to each other. The center platform was a triangle with 9-cm side-length. Each mouse was placed at the end of one arm, with its head directed to the walls, and allowed to freely explore the apparatus for 5 min. Sequential alternations in entering the arms were recorded by Time YM2.

Measurement of thermal hyperalgesia. A measurement of thermal hyperalgesia was performed as described previously (Imai et al., 2013) with minor modifications. To assess the sensitivity to thermal stimulation, each of the hind paws of the mice was tested individually using a thermal stimulus apparatus (model 33 Analgesia Meter; IITC/Life Science Instruments, Woodland Hills, CA, USA). The intensity of the thermal stimulus was adjusted to achieve an average baseline paw withdrawal latency of approximately 7 to 10 s in naive mice. Only quick hind paw movements (with or without licking of hind paws) away from the stimulus were considered to be a withdrawal response. The latency of paw withdrawal after the thermal stimulus was determined as the average of 3 trials per paw on each side.

Measurement of tactile allodynia. A measurement of tactile allodynia was performed as described previously (Imai et al., 2013) with minor modifications. To quantify the

sensitivity to a tactile stimulus, paw withdrawal in response to a tactile stimulus was measured using von Frey filaments (North Coast Medical, Inc., Morgan Hill, CA, USA) with a bending force of 0.02 g or 0.16 g. The von Frey filament was applied to the plantar surface of the hind paw for 3 sec, and this was repeated 3 times at intervals of at least 5 sec. Each of the hind paws was tested individually. Paw withdrawal in response to a tactile stimulus was evaluated by scoring as follows: 0, no response; 1, a slow and slight withdrawal response; 2, a slow and prolonged flexion withdrawal response (sustained lifting of the paw) to the stimulus; 3, a quick withdrawal response away from the stimulus without flinching or licking; 4, an intense withdrawal response away from the stimulus with brisk flinching and/or licking. The latency of paw withdrawal in response to a tactile stimulus was determined as the average of 2 trials per paw on each side.

Golgi-Cox staining. Golgi-Cox staining was done using a Rapid GolgiStain Kit (FD NeuroTechnologies) according to the protocol provided by the manufacturer, with minor modifications. The brain was removed from the skull without any perfusion, and then sectioned (100 μm) on a cryostat. After sections were mounted on cover slips, they were examined and photographed using an Axiovert 40 CFL microscope (Zeiss) equipped with a camera.

Cell and tissue morphometrics. Analysis of DCX-positive immature neurons was conducted from the 3D reconstruction of Z stack confocal images. The 2D projection images were used for further analysis. Twelve cells in total (3 cells / section x 4 sections) were picked per mouse and 4 mice from each group were used for the analysis. Golgi-stained neurons were analyzed from 2D images. Twelve sparse and

well-impregnated cells (3 cells / section x 4 sections) were selected per mouse and 3 mice from each group were used. The thickness of the immunostained area was measured at 6 different locations per section; 3 mice from each group were used. Images were traced and analyzed manually using GIMP (http://www.gimp.org) and ImageJ (http://rsbweb.nih.gov/ij). Maximum dendritic span of DG neurons and of the basal portion of CA1 neurons was measured as the angle between the two fartherst ends of the dendritic arborization and the center of the soma (see Figure S5C in Supplemental Information). For the apical portion of CA1 neurons, the same dendritic span measurement was conducted but stratum radiatum-oriented dendrites were excluded from the analysis. Dendritic complexity was measured using the Sholl analysis plugin for ImageJ (http://labs.biology.ucsd.edu/ghosh/software/index.html).

Voltage-sensitive dye imaging. *Slice preparation.* Hippocampal slices (400 μm) were prepared from 12-13-week-old male mice, decapitated under deep ether or isoflurane anesthesia. The brains were removed and cooled in ice-cold artificial cerebrospinal fluid (ACSF; 124 mM NaCl, 2.5 mM KCl, 2 mM $CaCl_2$, 2 mM $MgSO_4$, 1.25 mM NaH_2PO_4, 26 mM $NaHCO_3$, and 10 mM glucose, pH 7.4) bubbled with 95% O_2:5% CO_2 gas. After cooling for 5 min, the hippocampus was dissected out along with the surrounding cortex and sliced into 400-μm transverse sections with a vibratome (Leica VT-1200). Following incubation in gassed ACSF for 3–5 min, each slice was transferred onto a fine-mesh membrane filter (Omni Pore membrane filter, JHWP01300; Millipore), held in place by a thin Plexiglas ring (inner diameter, 11 mm; outer diameter, 15 mm; thickness, 1–2 mm). These slices were transferred to a moist chamber continuously supplied with a humidified O_2/CO_2 gas mixture. The temperature was held at 32 °C for 1 h, and after a further 1-h incubation at room

temperature the slices were stained for 25 min with 100 µl of VSD solution (0.2 mM di-4-ANEPPS (Molecular Probes) in 2.5% ethanol, 0.13% Cremaphor EL (Sigma), 1.17% distilled water, 48.1% FBS, and 48.1% ACSF). The slices were subjected to experiments after at least a 1-h incubation at room temperature following VSD washout.

Optical recording. The Plexiglas ring supporting each slice (see above) was placed in an immersion-type recording chamber. Slices were continuously perfused with prewarmed (31 °C) and oxygenated ACSF (bubbled with a 95% O_2:5% CO_2 gas mixture) at a rate of 1 ml/min. Custom laboratory-designed epifluorescence optics, used to view the slices during experiments, consisted of a custom-made objective lens (Olympus MYCAM 5x/0.6 WI; the final magnification of the system was x 5) and a Leica Microsystems MZ-APO (f = 55 mm ×1.0) projection lens. Excitation light was provided by a halogen lamp source (150 W; MHW-G150LR; Moritex) projected through an excitation filter ($\lambda = 530 \pm 10$ nm) and reflected onto the hippocampal slice by a dichroic mirror ($\lambda = 575$ nm). Emission fluorescence from the slice passed through an emission filter ($\lambda > 590$ nm) and was projected onto a C-MOS imager (MiCAM Ultima; BrainVision). The intensity of fluorescence emitted by the slice prior to stimulation was averaged and used as reference intensity (F_0). The fractional change in fluorescence [$\Delta F_{(t)} = F_{(t)} - F_0$] was normalized to the F_0 ($\Delta F/F_0$), and this value was used as the optical signal. Optical signals referred to below represent signals filtered in spatial and temporal dimensions with a digital Gaussian kernel of 5x5x3 (horizontal x vertical x temporal; $\sigma \approx 1$). We analyzed optical signals offline using a procedure developed for Igor Pro (WaveMetrics). At a wavelength of 610 nm, VSD fluorescence decreases in response to the depolarization of the cell membrane. To fit the polarity of the response to conventional membrane potential changes, we

expressed the optical signal in a polarity that matched the membrane potential change. For example, decreased fluorescence, which corresponds to depolarization, was represented as a positive deflection. Electrical stimulations (200 μA, bipolar 200 μsec) were applied with constant current pulses (A395, WPI) through a glass microcapillary tube (5 μm inner diameter; filled with ACSF) placed either on Schaffer collateral afferents in the CA3/CA1 border of CA1, on the granule cell layer to stimulate the mossy fiber pathway, or in the molecular layer of the upper blade in the dentate gyrus. The stimulation was applied with at least 20-sec intervals.

Supplemental References

Burgess, A., Vigneron, S., Brioudes, E., Labbé, J. C., Lorca, T., and Castro, A. (2010). Loss of human Greatwall results in G2 arrest and multiple mitotic defects due to deregulation of the cyclin B-Cdc2/PP2A balance. Proc. Natl. Acad. Sci. USA *107*, 12564-12569.

Gavet, O., and Pines, J. (2010). Progressive activation of CyclinB1-Cdk1 coordinates entry to mitosis. Dev. Cell *18*, 533-543.

Imai, S., Ikegami, D., Yamashita, A., Shimizu, T., Narita, M., Niikura, K., Furuya, M., Kobayashi, Y., Miyashita, K., Okutsu, D., et al. (2013). Epigenetic transcriptional activation of monocyte chemotactic protein 3 contributes to long-lasting neuropathic pain. Brain *136*, 828-843.

Kanno, J., Aisaki, K., Igarashi, K., Nakatsu, N., Ono, A., Kodama, Y., and Nagao, T. (2006). "Per cell" normalization method for mRNA measurement by quantitative PCR and microarrays. BMC Genomics *7*, 64.

Tanemura, K., Murayama, M., Akagi, T., Hashikawa, T., Tominaga, T., Ichikawa, M., Yamaguchi, H., and Takashima, A. (2002). Neurodegeneration with tau accumulation

in a transgenic mouse expressing V337M human tau. J. Neurosci. *22*, 133-141.

Tatebayashi, Y., Miyasaka, T., Chui, D.H., Akagi, T., Mishima, K., Iwasaki, K., Fujiwara, M., Tanemura, K., Murayama, M., Ishiguro, K., et al. (2002). Tau filament formation and associative memory deficit in aged mice expressing mutant (R406W) human tau. Proc. Natl. Acad. Sci. USA *99*, 13896-13901.